Forschungszentrum Karlsruhe
in der Helmholtz-Gemeinschaft

Wissenschaftliche Berichte
FZKA 7309

High Temperature Creep-Fatigue Structural Design Criteria for Fusion Components Built from EUROFER 97

Final Report:
TW2-TTMS-005b, D1
TW5-TTMS-005, D7

J. Aktaa, M. Weick, M. Walter

Institut für Materialforschung
Programm Kernfusion
Association Forschungszentrum Karlsruhe/EURATOM

August 2007

Forschungszentrum Karlsruhe

in der Helmholtz-Gemeinschaft

Wissenschaftliche Berichte

FZKA 7309

High temperature creep-fatigue structural design criteria for fusion components built from EUROFER 97

Final Report:

TW2-TTMS-005b, D1

TW5-TTMS-005, D7

J. Aktaa, M. Weick, M. Walter

Association Forschungszentrum Karlsruhe/EURATOM

Programm Kernfusion

Institut für Materialforschung

Forschungszentrum Karlsruhe GmbH, Karlsruhe

2007

Für diesen Bericht behalten wir uns alle Rechte vor

Forschungszentrum Karlsruhe GmbH
Postfach 3640, 76021 Karlsruhe

Mitglied der Hermann von Helmholtz-Gemeinschaft
Deutscher Forschungszentren (HGF)

ISSN 0947-8620

urn:nbn:de:0005-073093

Hochtemperatur-Auslegungsregeln für Kriech-Ermüdung von Fusionskomponenten aus EUROFER 97

Zusammenfassung

Die Hochtemperaturregeln für Kriech-Ermüdung der bereits etablierten ASME- und RCC-MR-Auslegungscodes wurden betrachtet, analysiert und für die Bewertung von aus EUROFER 97 gefertigten Bauteilen angepasst. Für die Verifikation der angepassten Regeln wurden isotherme Zwei-Stufen-Ermüdungs-, thermo-mechanische Ermüdungs- und isotherme mehrachsige Ermüdungsversuche durchgeführt und ausgewertet. Dabei wurde festgestellt, dass die herkömlichen Auslegungsregeln nicht ohne weiteres anwendbar auf EUROFER 97 sind. Sie können die beobachtete starke Lebensdauerabnahme unter thermo-mechanischen und mehrachsigen zyklischen Belastungen nicht erfassen, was hauptsächlich auf das unterschiedliche zyklische Entfestigungsverhalten unter diesen Belastungen im Vergleich zur isothermen einachsigen Belastung zurückgeführt wird. Aus diesem Grund wurden die Regeln durch die Herleitung neuer Ermüdungs-Auslegungskurven unter Berücksichtigung des zyklischen Entfestigungseinflusses modifiziert. Dabei wurde ein Schädigungsmodell verwendet, das zuletzt zur Beschreibung der Degradation von EUROFER 97 unter Kriech-Ermüdungsbelastungen entwickelt wurde. Auch wenn die verbesserten Regeln hinreichend bei der Betrachtung der Verifikationsversuche waren, werden weitere Verifikationen empfohlen.

Abstract

High temperature creep-fatigue design rules already established in the ASME and RCC-MR codes have been reviewed, analysed and reformulated for the assessment of components built from EUROFER 97. For the verification of the rules isothermal two-steps fatigue, thermo-mechanical fatigue and isothermal multiaxial fatigue tests have been performed and evaluated. It has been found that the conventional design rules are not straightforward applicable for EUROFER 97. They can not cover the strong lifetime reduction observed under thermo-mechanical and multiaxial cyclic loadings which has been mainly attributed to the different cyclic softening behaviour under these loading modes in comparison to isothermal uniaxial loading. Hence, the rules have been modified by deriving new fatigue design curves taking into account cyclic softening effects. Thereby, a damage model recently developed to describe the deterioration of EUROFER 97 under creep fatigue loading has been used. Even the improved rules have been sufficiently conservative when considering the verification tests performed further verifications are recommended.

TABLE OF CONTENTS

1 Introduction 1

2 Creep-fatigue evaluation rules 1
2.1 Damage equation 1
2.2 Equivalent strain range 3
2.2.1 ASME-Code 3
2.2.2 RCC-MR Code 5
2.2.3 Comparison between ASME and RCC-MR Codes 5
2.3 Design fatigue curves 6
2.4 Stress-to-rupture curves 6
2.5 Allowable total creep-fatigue damage 6

3 Application of the rules to EUROFER 97 7

4 Verification experiments 10
4.1 Isothermal two steps LCF experiments 10
4.1.1 Experimental 11
4.1.2 Results 12
4.2 Thermomechanical fatigue experiments 14
4.2.1 Experimental 14
4.2.2 Results 14
4.3 Isothermal multi-axial fatigue experiments 17
4.3.1 Experimental details 17
4.3.2 Experimental results 20

5 Improved rules for EUROFER 97 25

6 Summary and outlook 29

7 Acknowledgment 30

8 References 30

1 Introduction

The reduced activation ferritic martensitic (RAFM) steel EUROFER 97 developed recently in the framework of EURATOM Fusion Technology programme is a potential candidate as a structural material for in-vessel components of future fusion power plants [1]. During planed operation structural materials of in-vessel plasma facing components, Blanket and Divertor, are subjected to cyclic thermo-mechanical loading and high irradiation doses which yield different types of lifetime limiting failure mechanisms: ratchetting, creep, fatigue and radiation induced loss in ductility and toughness.

Within our activities in the EFDA Technology Work programme with the reference TTMS-005 “Rules for Design, Fabrication and Inspection” structural design criteria for components built from EUROFER 97 will be developed and qualified. Our investigations are focused on high temperature rules, particularly those for preventing creep, fatigue and creep/fatigue interaction, not yet considered and implemented in the current ITER Structural Design Criteria for In-Vessel Components (SDC-IC) [2]. Therefore we started evaluating the high temperature rules of the current design codes well established for nuclear applications: ASME Boiler and Pressure Vessels Code, Code Case N-47 and the French RCC-MR code, RB 3200 and RC 3200. For the evaluation various verification experiments have been planed and performed. The aim of the evaluation is to determine whether the well established rules provide a sufficient safety margin when they are applied to EUROFER 97 structures and if they do so how much their conservatism amounts. In parallel a coupled deformation damage model for creep-fatigue interaction has been developed [3] which should provide a best estimated lifetime prediction and thus help in removing the unnecessary conservatism the design rules might have.

In this report, a brief overview about the creep-fatigue evaluation rules of the ASME-BPV and RCC-MR codes and about how they can be applied to EUROFER 97 structures will be firstly given. Thereafter the verification experiments performed are described and their results are presented and discussed particularly from point of view of the conventional design rules. Based on this discussion and the knowledge gathered so far recommendations for new design rules and further verification experiments are concluded.

2 Creep-fatigue evaluation rules

In the ASME-BPV (Code Case N-47, T-1400) and RCC-MR (RB 3262.12) codes similar rules are used for design against creep, fatigue and creep-fatigue interaction. They are based on the compliance of a damage equation for its application numerous criteria are proposed.

2.1 Damage equation

To accept a design subjected to service loadings yielding creep and fatigue damage, including hold time and strain rate effects, the linear summation of fatigue and creep damage shall not exceed the allowable total creep-fatigue damage D' satisfying the following relation:

$$\sum_{j=1}^{p}\left(\frac{n}{N_d}\right)_j + \sum_{k=1}^{q}\left(\frac{\Delta t}{T_d}\right)_k \le D' \qquad (2.1)$$

where

p = number of different cycle types required to define the cyclic strain history for the specified service life. Each cycle type is uniquely defined by its equivalent mechanical strain range $\Delta\varepsilon$ and the maximum material temperature occurring during the cycle.

$(n)_j$ = number of applied repetitions of cycle type j.

$(N_d)_j$ = number of design allowable cycles for cycle type j determined from one of the design fatigue curves corresponding to the maximum material temperature occurring during the cycle. The design fatigue curves were determined from completely reversed loading conditions at strain rates greater than, or equal to those noted on the curves.

q = number of time intervals (each with a unique stress-temperature combination) needed to represent the specified elevated temperature service life at the point of interest for the creep damage calculation.

$(T_d)_k$ = allowable time duration determined from stress-to-rupture curves for a given stress and the maximum temperature at the point of interest and occurring during the time interval k. For inelastic analysis the following equivalent stress quantity should be used

$$\sigma_e = \bar{\sigma}\exp\left[C\left(\frac{J_1}{S_s}-1\right)\right] \qquad \text{ASME} \qquad (2.2)$$

$$\sigma_e = 0.867\bar{\sigma} + 0.133J_1 \text{.....RCC-MR} \qquad (2.3)$$

where

$$J_1 = \sigma_1 + \sigma_2 + \sigma_3$$

$$S_s = \left[\sigma_1^2 + \sigma_2^2 + \sigma_3^2\right]^{1/2}$$

$$\bar{\sigma} = \frac{1}{\sqrt{2}}\left[(\sigma_1-\sigma_2)^2 + (\sigma_2-\sigma_3)^2 + (\sigma_1-\sigma_3)^2\right]^{1/2}$$

and σ_i are the principal stresses. The constant C in equation 2.2 is material dependent (equal 0.24 for types 304 and 316 stainless steels and 0.0 for Alloy 800H and 2-1/4 Cr-1 Mo steel). The allowable time duration is determined by entering the stress-time to rupture curves at that stress value determined

by dividing the maximum equivalent stress (at the point of interest during the time interval k) by the factor K' which is in general material dependent. However K' is specified as constant for all materials and equal 0.67 in the ASME Code and 0.9 in the RCC-MR Code.

$(\Delta t)_k$ = duration of the time interval k. The sum of the q time intervals must equal or exceed the total specified elevated temperature service life.

For the evaluation of the fatigue damage portion of any cycle type j, first term in equation 2.1, the mechanical strain range and the material specific design fatigue curves are required. In addition, to determine the creep damage fraction the material specific stress-to-rupture curves are necessary. Finally for the examination of 2.1 the material specific values of the allowable total creep-fatigue damage D' should be known.

2.2 Equivalent strain range

2.2.1 ASME-Code

In the ASME Code, Code Case N-47, T-1413 the equivalent mechanical strain range $\Delta\varepsilon$ is defined equal $\Delta\varepsilon_{\max}$ which is computed as follows:

Step 1. Calculate all strain components for each point i in time (ε_{11i}, ε_{22i}, ε_{33i}, ε_{12i}, ε_{23i}, ε_{31i}) for the complete cycle.

Step 2. Select a point when conditions are at an extreme for the cycle, either maximum or minimum. Refer to this time point by a subscript o.

Step 3. Calculate the history of the change in strain components by subtracting the values at the time o from the corresponding components at each point in time i during the cycle.

$$\Delta\varepsilon_{11i} = \varepsilon_{11i} - \varepsilon_{11o}$$
$$\Delta\varepsilon_{22i} = \varepsilon_{22i} - \varepsilon_{22o}$$
$$etc;$$

Step 4. Calculate the equivalent strain range for each point in time as:

$$\Delta\varepsilon_{eq.i} = \frac{\sqrt{2}}{2(1+\upsilon^*)}\Big[\left(\Delta\varepsilon_{11i} - \Delta\varepsilon_{22i}\right)^2 + \left(\Delta\varepsilon_{22i} - \Delta\varepsilon_{33i}\right)^2 + \left(\Delta\varepsilon_{33i} - \Delta\varepsilon_{11i}\right)^2 + 6\left(\Delta\varepsilon_{12i}^2 + \Delta\varepsilon_{23i}^2 + \Delta\varepsilon_{31i}^2\right)\Big]^{1/2} \quad (2.4)$$

where

$\upsilon^* = 0.5$ when using the rules in inelastic analysis

$\upsilon^* = 0.3$ when using the rules in elastic analysis

Step 5. Define $\Delta\varepsilon_{\max}$ as the maximum value of the above calculated equivalent strain ranges $\Delta\varepsilon_{eq.i}$

The above five step procedure may be used regardless of whether principal strain change directions or not. When principal strains do not rotate the ASME Code provides in Code Case N-47, T-1414 an alternative calculation method:

Step 1. Calculate all strain components for each point i in time (ε_{11i}, ε_{22i}, ε_{33i}, ε_{12i}, ε_{23i}, ε_{31i}) for the complete cycle.

Step 2. Determine the principal strains (ε_1, ε_2, ε_3) versus time for the cycle

Step 3. At each point in time determine the strain differences $\varepsilon_1 - \varepsilon_2$, $\varepsilon_2 - \varepsilon_3$, $\varepsilon_3 - \varepsilon_1$.

Step 4. Select a point when conditions are at an extreme for the cycle, either maximum or minimum. Refer to this time point by a subscript o.

Step 5. Determine the history of the change in strain differences by subtracting the values at the time o from the corresponding values at each point in time i during the cycle. Designate these strain difference changes as

$$\Delta(\varepsilon_1 - \varepsilon_2)_i = (\varepsilon_1 - \varepsilon_2)_i - (\varepsilon_1 - \varepsilon_2)_o$$
$$\Delta(\varepsilon_2 - \varepsilon_3)_i = (\varepsilon_2 - \varepsilon_3)_i - (\varepsilon_2 - \varepsilon_3)_o$$
$$\Delta(\varepsilon_3 - \varepsilon_1)_i = (\varepsilon_3 - \varepsilon_1)_i - (\varepsilon_3 - \varepsilon_1)_o$$

Step 6. For each point in time i calculate the equivalent strain range as

$$\Delta\varepsilon_{eq.i} = \frac{\sqrt{2}}{2(1+\upsilon^*)}\left\{\left[\Delta(\varepsilon_1 - \varepsilon_2)_i\right]^2 + \left[\Delta(\varepsilon_2 - \varepsilon_3)_i\right]^2 + \left[\Delta(\varepsilon_3 - \varepsilon_1)_i\right]^2\right\}^{1/2} \quad (2.5)$$

where

$\upsilon^* = 0.5$ when using the rules in inelastic analysis

$\upsilon^* = 0.3$ when using the rules in elastic analysis

Step 7. Define $\Delta\varepsilon_{\max}$ as the maximum value of the above calculated equivalent strain ranges $\Delta\varepsilon_{eq.i}$

2.2.2 RCC-MR Code

In the RCC-MR Code (RB 3227.9) a similar method to that in the ASME Code is proposed for the determination of the equivalent mechanical strain range $\Delta\varepsilon$. Therefore $\Delta\varepsilon$ is defined equal $\overline{\Delta\varepsilon}$ which is calculated as follows:

Step 1. At each instant (t) of the cycle, calculate the components of the strain tensor $\boldsymbol{\varepsilon}(t)$ at the point examined: $\varepsilon_{11}(t),\ \varepsilon_{22}(t),\ \varepsilon_{33}(t),\ \varepsilon_{12}(t),\ \varepsilon_{23}(t),\ \varepsilon_{31}(t)$

Step 2. Calculate the strain range tensor $\boldsymbol{\varepsilon}(t,t')$ for each pair of instants (t) and (t') of the cycle. The components of tensor $\boldsymbol{\varepsilon}(t,t')$ are equal to the difference between the components of the tensors $\boldsymbol{\varepsilon}(t)$ and $\boldsymbol{\varepsilon}(t')$:

$$\boldsymbol{\varepsilon}(t,t') = \boldsymbol{\varepsilon}(t) - \boldsymbol{\varepsilon}(t')$$

Step 3. Calculate the equivalent scalar strain range $\overline{\varepsilon(t,t')}$ between the states (t) and (t') using one of the following formulae:

$$\overline{\varepsilon(t,t')} = \frac{\sqrt{2}}{3}\left\{\left[\varepsilon_{11}(t,t') - \varepsilon_{22}(t,t')\right]^2 + \left[\varepsilon_{22}(t,t') - \varepsilon_{33}(t,t')\right]^2 + \left[\varepsilon_{33}(t,t') - \varepsilon_{11}(t,t')\right]^2 + 6\left(\varepsilon_{12}^2(t,t') + \varepsilon_{23}^2(t,t') + \varepsilon_{31}^2(t,t')\right)\right\}^{1/2} \quad (2.6)$$

$$\overline{\varepsilon(t,t')} = \frac{\sqrt{2}}{3}\left\{\left[\varepsilon_1(t,t') - \varepsilon_2(t,t')\right]^2 + \left[\varepsilon_2(t,t') - \varepsilon_3(t,t')\right]^2 + \left[\varepsilon_3(t,t') - \varepsilon_1(t,t')\right]^2\right\}^{1/2} \quad (2.7)$$

where

$\varepsilon_{11}(t,t'),\ \varepsilon_{22}(t,t')\ldots$ are the components of the tensor $\boldsymbol{\varepsilon}(t,t')$ and

$\varepsilon_1(t,t'),\ \varepsilon_2(t,t'),\ \varepsilon_3(t,t')$ are the principal components of this tensor.

Step 4. For the cycle examined, the strain range is equal to the greatest of the quantities $\overline{\varepsilon(t,t')}$ calculated for each pair of instants (t) and (t') of the cycle:

$$\overline{\Delta\varepsilon} = \max_{t,t'}\left[\overline{\varepsilon(t,t')}\right] \quad (2.8)$$

This method was adopted by the ITER SDC-IC and can be retrieved in Appendix B under B 2630 [2].

2.2.3 Comparison between ASME and RCC-MR Codes

When comparing the methods of ASME and RCC-MR Codes it can be pinpointed that they are similar and would yield, when they are applied correctly, the same results. However the

selection of the point in time when conditions are at an extreme for the cycle, step 2 of T-1413 and step 4 of T-1414, respectively, is not a straightforward task particularly in inelastic analysis which might be a weak point for the ASME method. On the other hand the use of the principal components of the strain tensor to calculate the equivalent strain range is in the ASME method strictly limited to the case where the directions of the principal strains do not rotate which is not the case in the RCC-MR method where the equations 2.6 and 2.7 are supposed to deliver the same values what they do not necessarily do when the directions of the principal strains rotate.

2.3 Design fatigue curves

Design fatigue curves for a material will be constructed according to the criteria of the ASME (Section III, Division 1 – Appendices, III-2200) and the RCC-MR (A3.GEN.23) codes in a similar ways. They are obtained from fatigue lifetime (number of cycles to rupture) data of uniaxial strain-controlled fatigue (low cycle fatigue, LCF) tests performed with a strain rate in the order of $10^{-3}\,\mathrm{sec}^{-1}$. A best fit to experimental data is obtained by applying the method of least squares to the logarithms of the strain range values. The design fatigue curves are then deduced from the best fit curve by applying a factor of 2 on strain range or a factor of 20 on cycles, whichever is the more conservative at each point. These factors are intended to cover effects such as those of the environment, the scale (between the material and the test specimen), surface finish and data scatter [4]. They in no case constitute a safety coefficient.

2.4 Stress-to-rupture curves

In the ASME as well as RCC-MR codes the stress-to-rupture curves to be used are derived from lifetime data of creep tests. They deliver for a given temperature and time the minimum stress value S_r which yields to rupture at the given temperature after the given time.

2.5 Allowable total creep-fatigue damage

Taking into account nonlinear damage accumulation effects the allowable total creep-fatigue damage is not specified in the ASME as well as in the RCC-MR code as constant equal to 1 but as a variable dependent on the creep and fatigue damage fractions, respectively. The dependence is given graphically in the form of a creep-fatigue interaction envelope, which shall not be exceeded by the sum of creep and fatigue damage fractions (left side in equation 2.1). This envelope is material specific and has to be derived on the base of experiments with variable creep and fatigue damage fractions. It assigns the minimums obtained for linear sums of creep and fatigue damage fractions calculated as specified on the left side of equation 2.1. Figure 2.1 gives the creep-fatigue interaction envelopes can be find in the ASME Code (Code Case N-47, Figure T-1420-2) and in the RCC-MR Code (A3.*x*S.58; *x*=1,2,3).

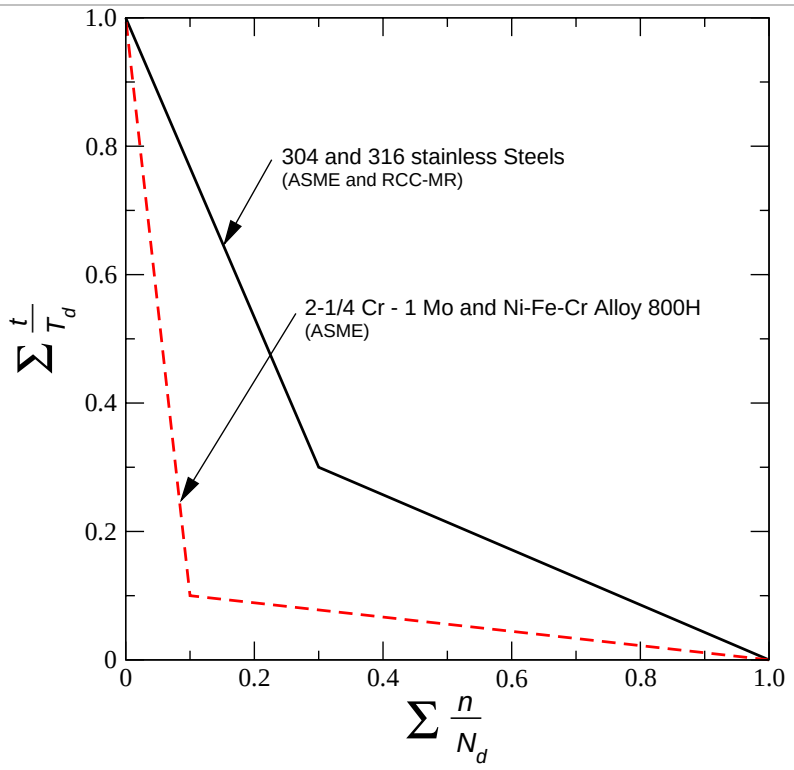

Figure 2-1 Creep-fatigue damage envelope

3 Application of the rules to EUROFER 97

To use the creep-fatigue rules illustrated in the previous section for the evaluation of components built from EUROFER 97 the necessary design fatigue and stress-to-rupture curves have to be obtained for this material. In addition, a creep-fatigue damage envelope which provides the allowable total damage values for EUROFER 97 has to be identified.

Following the codes instructions given in 2.3 the design fatigue curves are constructed by fitting the relation

$$\Delta\varepsilon = a_1 + a_2 N_f^{a_3} \tag{3.1}$$

to the isothermal low cycle fatigue data of EUROFER 97 (mechanical strain range $\Delta\varepsilon$ vs. number of cycles to failure N_f) and applying the appropriate factors what yields the following formula for the design fatigue curves (mechanical strain range $\Delta\varepsilon$ vs. number of allowable cycles N_d):

$$\Delta\varepsilon = \min\left\{0.5\left(a_1 + a_2 N_d^{a_3}\right), a_1 + a_2\left(20 * N_d\right)^{a_3}\right\} \tag{3.2}$$

The resulting values of the temperature dependent parameters a_1, a_2 and a_3 for EUROFER 97 are listed in Table 3-1 whereas the quality of the fits is demonstrated in Figure 3-1. In Figure 3-2 the design fatigue curves of EUROFER 97 obtained accordingly are plotted.

Table 3-1: Parameters of equation 3.2 determined for EUROFER 97

Temperature in °C	a_1	a_2	a_3
20	3.84×10^{-3}	0.83	-0.58
450	3.84×10^{-3}	1.06	-0.68
550	3.20×10^{-3}	1.16	-0.68
650	2.88×10^{-3}	1.92	-0.73

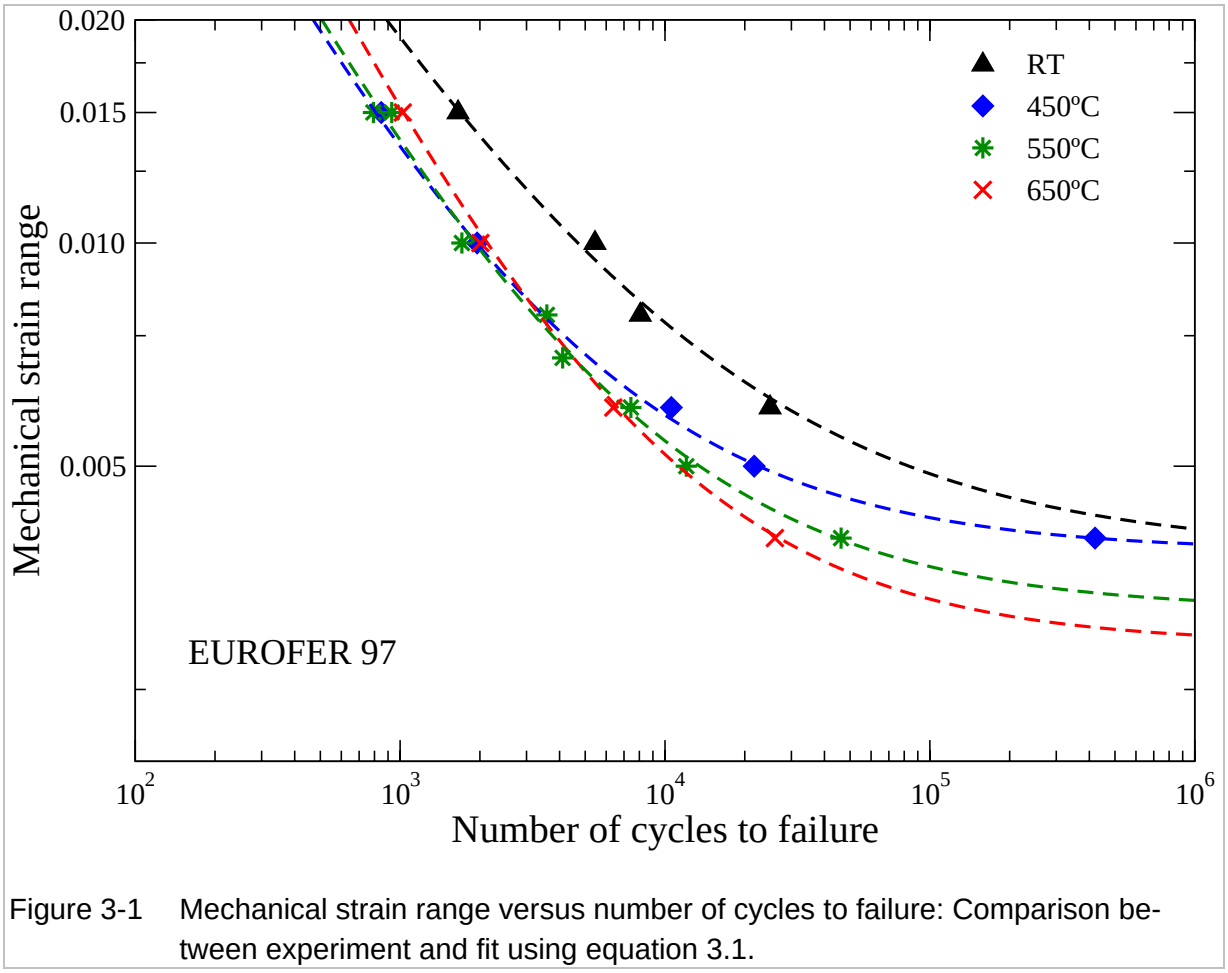

Figure 3-1 Mechanical strain range versus number of cycles to failure: Comparison between experiment and fit using equation 3.1.

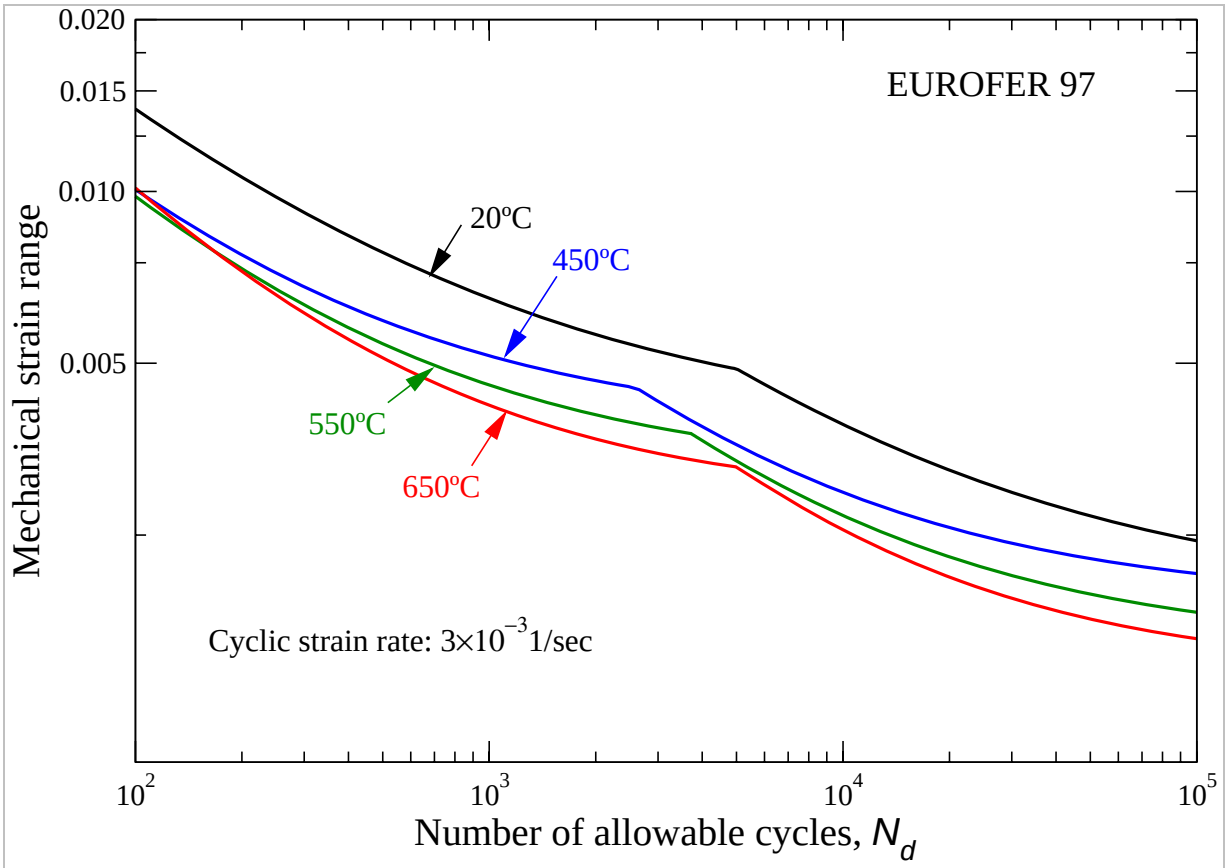

Figure 3-2 Design fatigue strain range for EUROFER 97

The stress-to-rupture curves are already determined in [5] on the base of creep lifetime data. Therefore the following relation between the minimum stress value S_r and the Larson-Miller-Parameter P is deduced (S_r in MPa)

$$S_r = 1936 - 88.452P + 0.888324P^2 \qquad (3.3)$$

where

$$P = (30 + \log(T_d)) * (\theta + 273)/1000$$

with T_d and θ denoting the allowable time in h (hours) and the temperature in °C, respectively. Figure 3-3 shows the stress-to-rupture curves of EUROFER 97 determined using equation 3.3 for different temperatures.

The creep-fatigue damage envelope suitable to EUROFER 97 has to be determined on the base of lifetime data of tests with different creep and fatigue damage fractions, like low cycle fatigue tests with different dwell times. Since the data available from this type of tests are not sufficient further tests, particularly with long dwell times will be performed in current activities in the EFDA Technology Work programme (TW5-TTMS-005 D9). However, as long as a creep-fatigue damage envelope for EUROFER 97 can not be determined, one might assume the most conservative envelope specified in the ASME Code for 2-1/4 Cr – 1 Mo and Ni-Fe-Cr Alloy 800H (see Figure 2-1) to be valid for EUROFER 97.

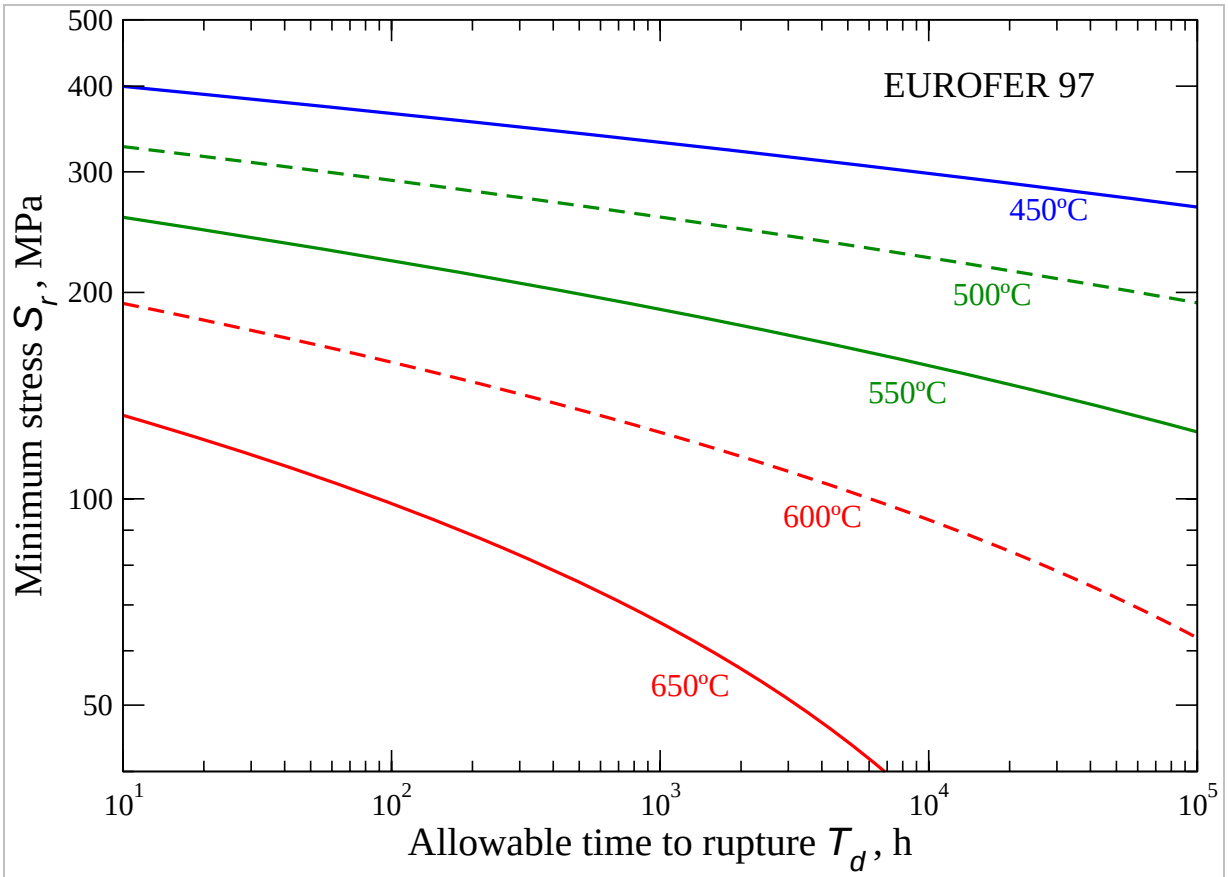

Figure 3-3 Stress-to-rupture curves for EUROFER 97

Hence the application of the creep-fatigue evaluation rule (equation 2.1) to components built from EUROFER 97 is possible but its qualification needs a comprehensive verification applying the rule to all possible loading scenarios first wall components of a fusion power plant might be exposed. Therefore numerous verification experiments have been conducted which will be described in details in the coming section.

4 Verification experiments

4.1 Isothermal two steps LCF experiments

The aim of this type of experiments is the investigation of non-linear damage accumulations which yield to sequence effects ignored by the creep-fatigue damage rule (equation 2.1) when applied to pure fatigue considering the allowable damage values given by the creep-fatigue damage envelopes in Figure 2.1:

$$\sum_{j=1}^{p}\left(\frac{n}{N_d}\right)_j \le 1 \qquad (4.1)$$

Sequence effects are observed for most materials whose fatigue data show that the sequence of high-low load cycles leads to a lower number of cycles to failure than the reverse

low-high cycles. To quantify these effects in the fatigue behaviour of EUROFER 97 isothermal two steps LCF experiments have been performed.

4.1.1 Experimental

The isothermal two steps experiments were carried out using radial polished round specimens (diameter d_0 = 8,8 mm, gauge length l_0 = 20 mm) that were fabricated from one plate in the as delivered state [6]. They were performed in a strain controlled manner (strain rate $\dot{\varepsilon} = 3\times10^{-3}$, ratio of minimum to maximum strain R = -1) at 450°C and 550°C, respectively, using a hydraulic testing machine by MTS (type 810 with a TestStar IIs controller) that is equipped with a quad elliptical heating chamber from R-I CONTROLS.

The load conditions were varied in the two steps experiments by changing the total strain amplitude $\Delta\varepsilon$ from 1.0 % to 0.6 % (or vice versa). The respective switch point was given by a variation of the number of cycles in the first step depending on a different ratio between the number of cycles and the number of cycles to failure ($n_\mathrm{j} / N_{f\,\mathrm{j}}$ with j as step number – $N_{f\,\mathrm{j}}$ determined in single-step experiments for the respective $\Delta\varepsilon_\mathrm{j}$). After changing the total strain amplitude, the test was continued by the second step until fracture. Figure 4-1 shows an example of the peak stress σ_o as a function of the number of cycles n in a test at a total strain amplitude of $\Delta\varepsilon$ = 1.0 % in the first step. From the curve, the material parameter $n_{d\,\mathrm{j}}$ (number of cycles to macroscopic damage where the curve leaves its linear behaviour because of a decreasing cross-section resulting from the fusion of micro-cracks to a macro-crack and the following crack propagation) can be determined. For comparison, the number of cycles to failure $n_{f\,\mathrm{j}}$ is determined at the peak stress value equal to the peak stress at $n_{d\,\mathrm{j}}$ decreased by 30 %.

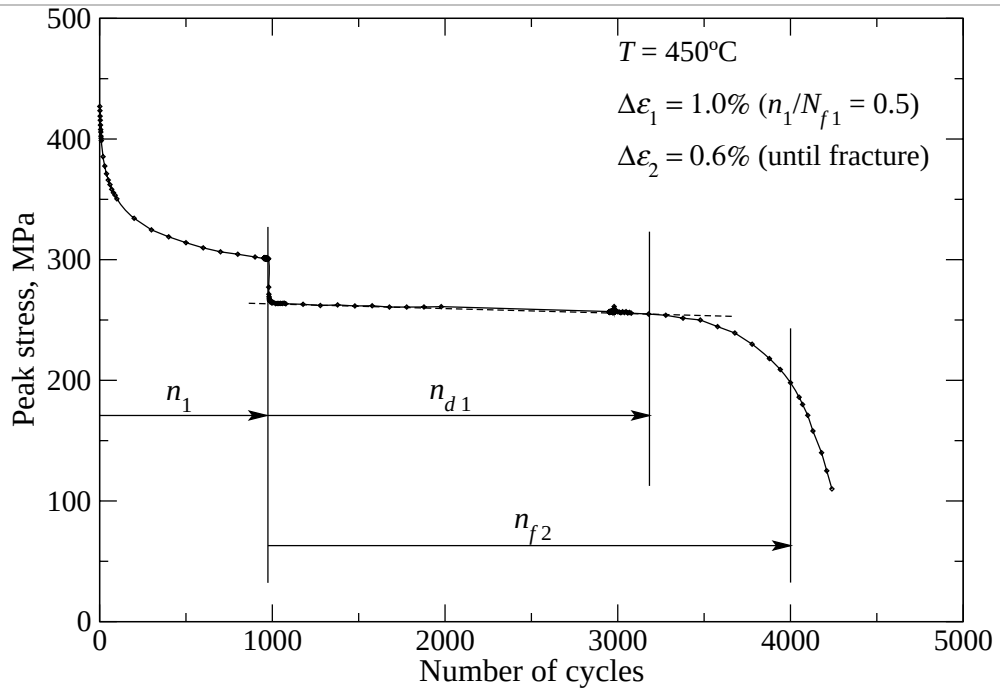

Figure 4-1 Peak stress vs. number of cycles, an example of a 2-step experiment, beginning with $\Delta\varepsilon_1$ = 1.0 % in the first step

4.1.2 Results

When plotting the results of the two steps experiments in a Palmgren-Miner diagram [7] (see Figure 4-2), non-linear damage accumulation can be recognized. Beginning with the high total strain amplitude ($\Delta\varepsilon_1$ = 1.0 %) leads to lifetimes shorter than those expected assuming linear damage accumulation, particularly with decreasing n_1 / N_{f1} ratio, i.e. $\sum n_j / N_{fj} < 1$. In contrast to this, starting with a low total strain amplitude ($\Delta\varepsilon_1$ = 0.6 %) leads to clearly longer lifetimes than those expected assuming linear damage accumulation, i.e. $\sum n_j / N_{fj} > 1$. Consequently, the allowable damage summation $\sum n_j / N_{fj}$ must be lower than the minimum value obtained from these experiments which is equal to 0.57 so far (s. Table 4-1). However when calculating the damage summation using the number of allowable cycles N_{dj} instead of N_{fj} according to equation 4.1 the allowable damage summation $\sum n_j / N_{dj}$ are greater than 1 and less than 11.2 (s. Table 4-1). This reveals that the creep-fatigue damage rule applied to pure fatigue (equation 4.1) is on the safe side and might even be too conservative when applied to EUROFER 97.

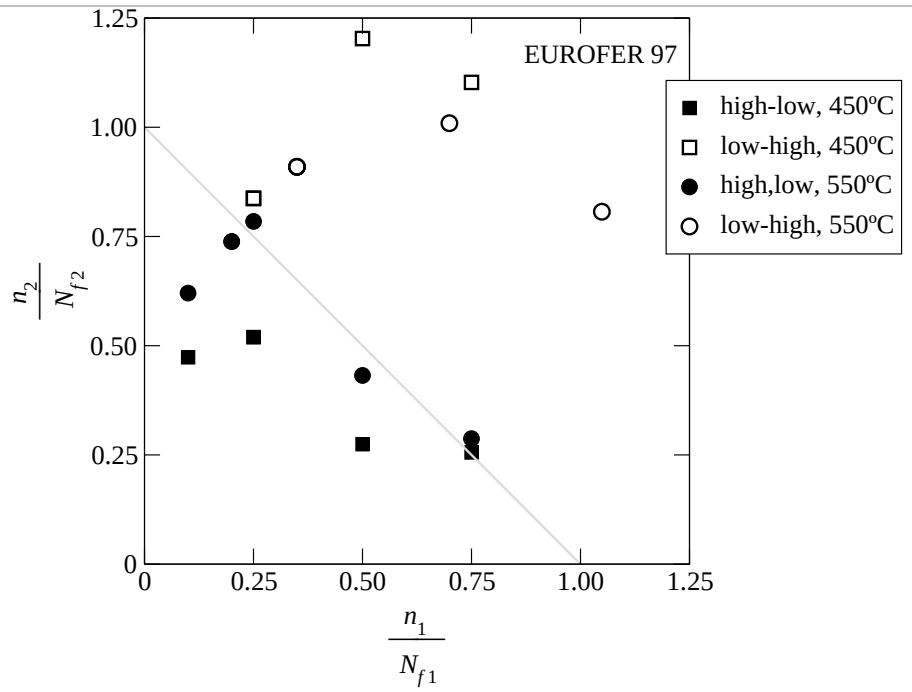

Figure 4-2 Results of the 2-step experiment, plotted in a Palmgren-Miner diagram

Table 4-1: Calculated damage summations for two steps experiments on EUROFER 97

Temperature in °C	Sequence	n_1 / N_{f1}	$\sum_j n_j / N_{fj}$	$\sum_j n_j / N_{dj}$
450	high-low	0.25	0.77	16.03
		0.50	0.77	15.81
		0.75	1.01	20.40
		0.10	0.57	12.06
	low-high	0.25	1.09	22.01
		0.50	1.70	34.63
		0.75	1.85	37.94
550	high-low	0.20	0.94	14.80
		0.25	1.03	16.40
		0.50	0.93	15.56
		0.75	1.04	17.87
		0.10	0.72	11.20
	low-high	0.35	1.26	21.69
		0.70	1.71	28.79
		1.05	1.86	30.43

4.2 Thermomechanical fatigue experiments

4.2.1 Experimental

The thermo-mechanical fatigue tests have been were performed on EUROFER 97 using cylindrical hollow specimens and the thermo-mechanical fatigue rig as described in [8]. During the test, the specimen, which is clamped between two stiff rods in a stiff load frame, is cooled and heated cyclically between the upper and lower temperatures starting from the mean temperature, at which the specimen initially is stress free. Due to clamping, the total strain of the specimen remains constant during the test and equal to 0 so that cooling and heating of the specimen result in induced out of phase mechanical strain and stress (Figure 4-3). The amplitude of induced mechanical load is varied from test to test by varying the upper temperature of the test.

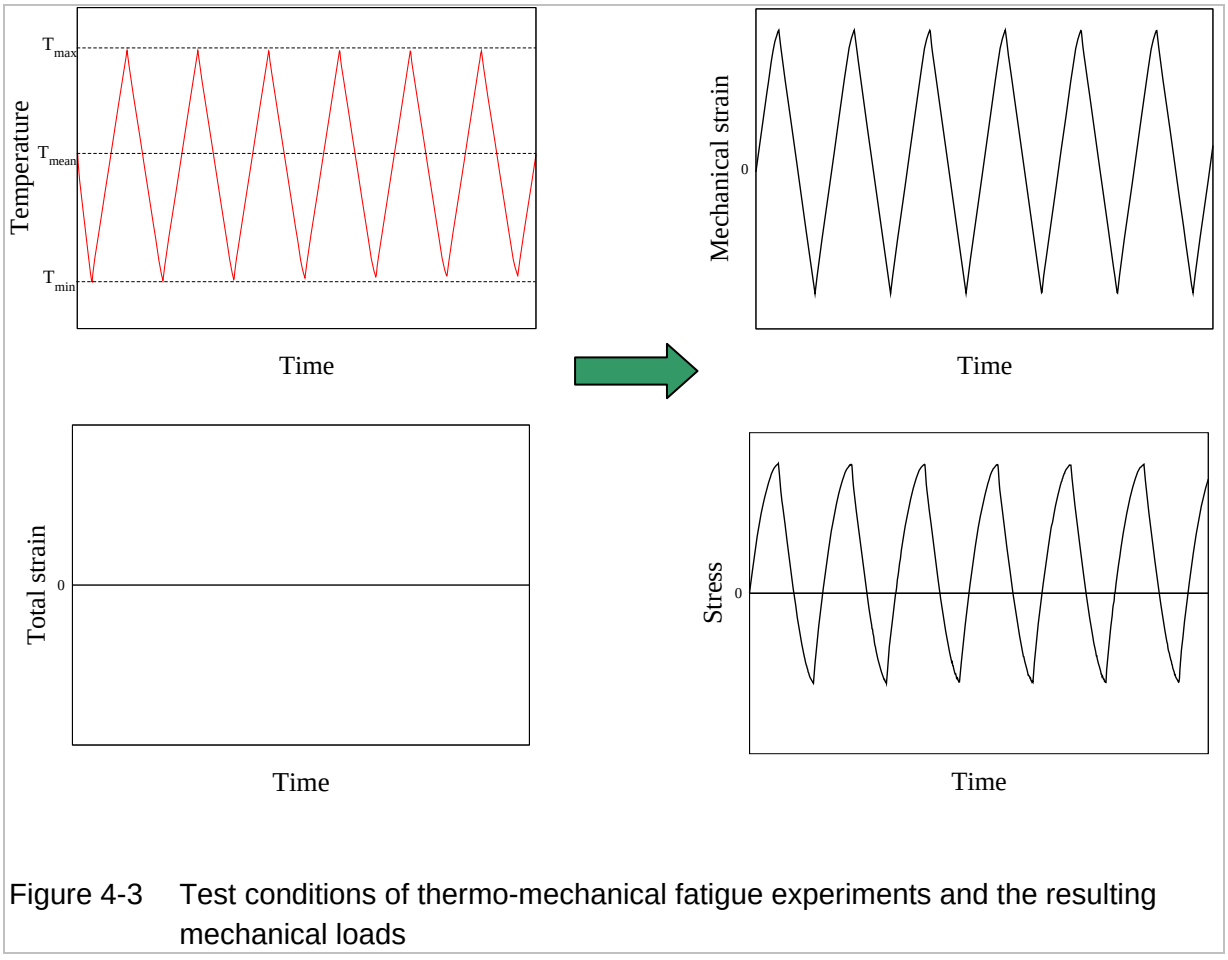

Figure 4-3 Test conditions of thermo-mechanical fatigue experiments and the resulting mechanical loads

4.2.2 Results

In a first evaluation, the mechanical strain range determined for the cycle at the half number of cycles to failure is plotted versus the number of cycles to failure and compared with the corresponding plots obtained from the isothermal fatigue tests (Fig. 4-4). For the same mechanical strain range, the thermo-mechanical fatigue tests show up to a factor of 20 lower numbers of cycles to failure than the isothermal fatigue tests. Consequently the fatigue lifetimes of thermo-mechanical fatigue tests lie very close to and even below the curve marking

the numbers of allowable cycles N_d as determined in section 3 for EUROFER 97 and corresponding to the highest temperature within the thermo-mechanical cycle. In addition, this difference between thermo-mechanical fatigue and isothermal fatigue test results for EUROFER 97 is much higher than the differences published in the literature for other materials [9].

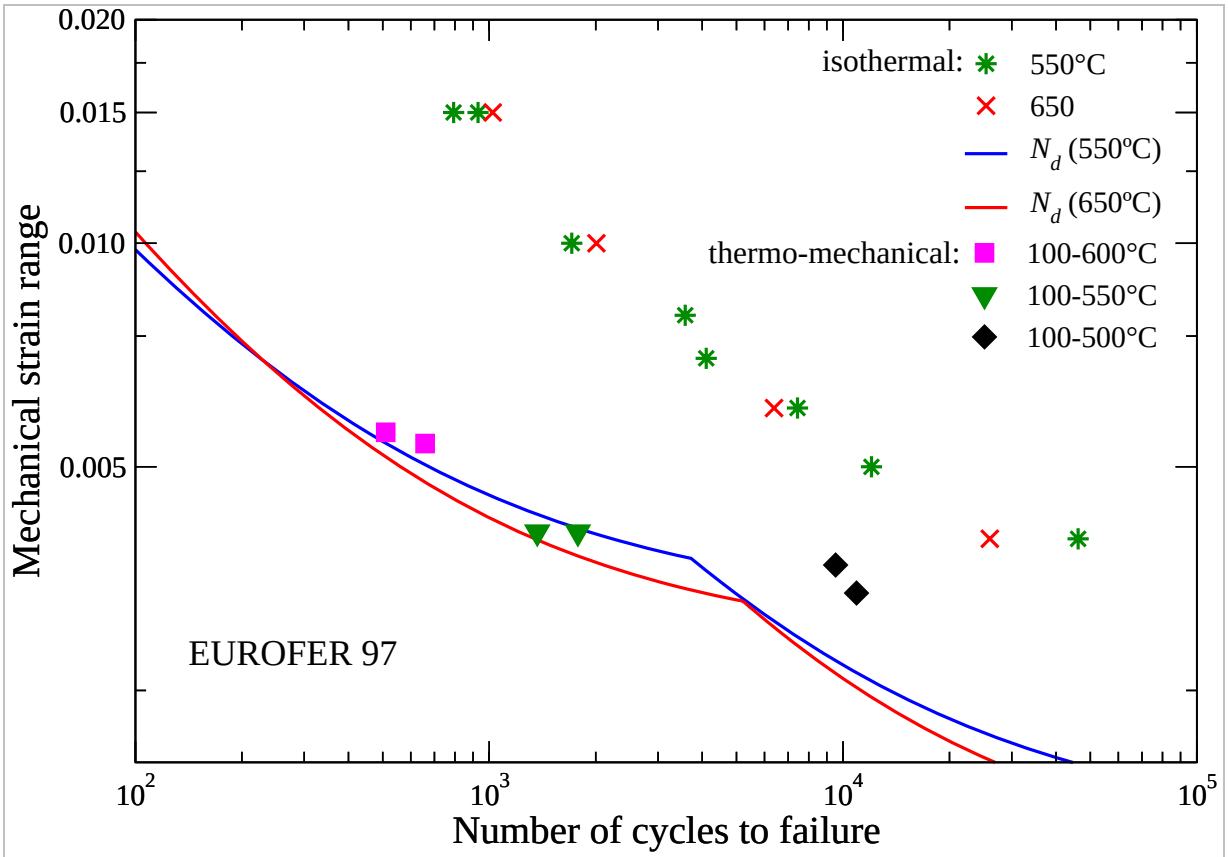

Figure 4-4 Results of thermo-mechanical fatigue tests in comparison to those of isothermal fatigue tests and the design curves derived from (mechanical strain range at the half number of cycles to failure vs. number of cycles to failure).

The thermo-mechanical fatigue tests are analyzed in a first step from the mechanical point of view in order to identify whether the highly reduced lifetime is an effect related to the test conditions or to the material or to both. When doing so it is recognized that the mechanical strain range determined and plotted in Fig. 4-4 for thermo-mechanical fatigue tests is actually that measured for the gauge length of the specimen, at which the temperature drops from its middle, where the temperature is controlled equal to the nominal value, to its ends. Depending on the nominal temperature, the temperature variation from the middle to the ends of the gauge length may amount to several tens of °C, so that the mechanical strain range at the middle of the gauge length, where the specimen fails, might be much higher than that measured for the total gauge length. In addition, this difference is expected to increase from cycle to cycle due to the cyclic softening behavior of EUROFER 97. This consideration gave us reason to perform finite element simulations to estimate the mechanical strain range at the middle of the gauge length.

The finite element simulations of the thermo-mechanical tests, details can be found in [10], showed that at the middle of the specimen a mechanical strain range higher than the value

measured as an average for the gauge length in the real test can be calculated. However, this maximum mechanical strain range is still lower than that corresponding to the experimentally observed fatigue life predicted on the base of isothermal fatigue data (Figure 4-5). Accordingly one may conclude that thermo-mechanical cycling of EUROFER 97 yields more fatigue damage than isothermal cycling with the same mechanical strain range. But before doing so, it should be ruled out that the progressive strain localization calculated at the middle of the thermo-mechanical fatigue specimen, caused by both temperature gradients in the specimen and cyclic softening behavior of the material, would yield to deformation instabilities and locally even higher fatigue loads. These deformation instabilities and the resulting higher local fatigue loads can not be correctly modeled by the geometric linear finite element simulations performed. However, they can be investigated performing either geometrically nonlinear simulations, which require development of additional tools, or thermo-mechanical fatigue tests with specimens of different geometries and buckling behavior, respectively [10].

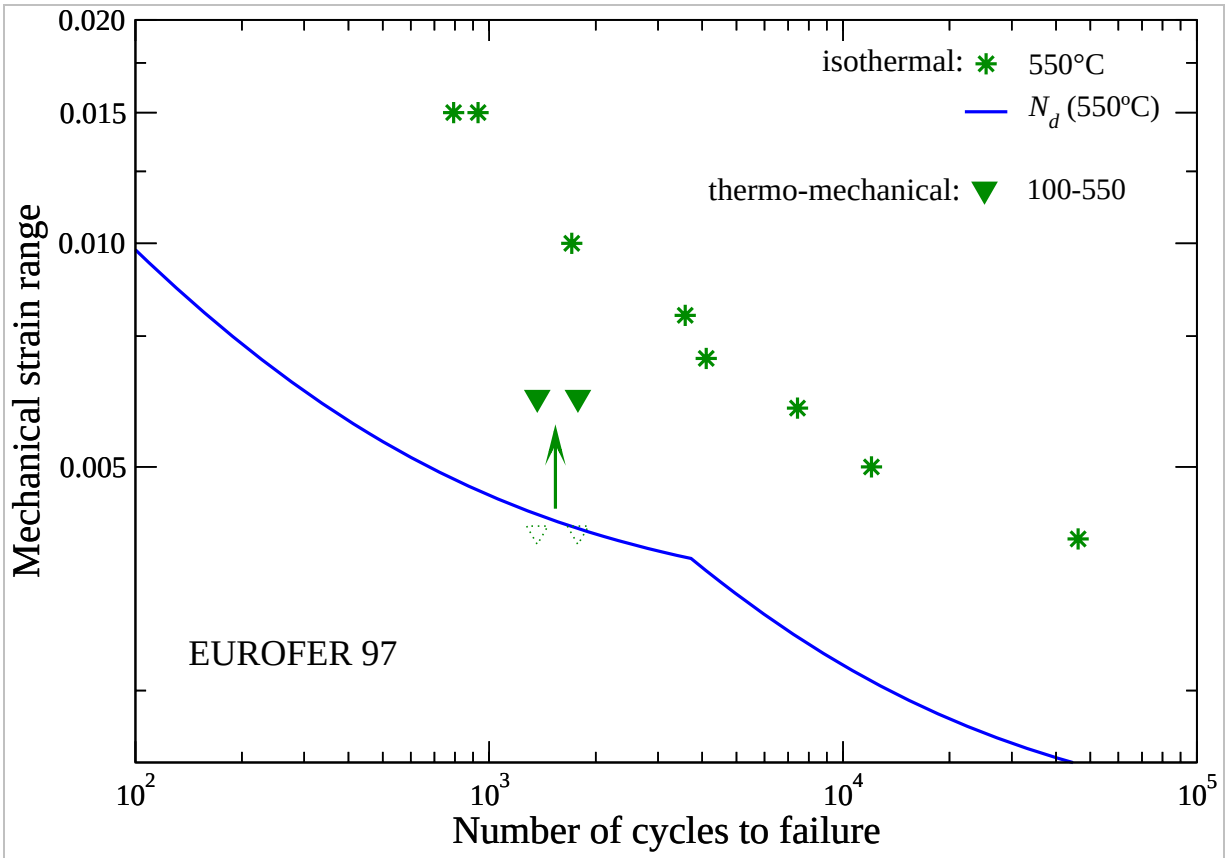

Figure 4-5 Maximum mechanical strain range at the half number of cycles to failure calculated using finite element simulations versus number of cycles to failure for thermo-mechanical fatigue tests in comparison to those of isothermal fatigue tests and the design curve derived therefrom.

4.3 Isothermal multi-axial fatigue experiments

Two types of strain controlled multiaxial fatigue tests have been performed on EUROFER 97 tube specimens:

1. Cyclic pull-push in axial and circumferential directions of the specimen and thus with fixed directions of principal stresses and strains (FPSS) at room temperature. The tests performed in that way will be called in the following FPSS tests.

2. Cyclic pull-push and alternating torsion in the axial direction of the specimens which yield the directions of the principal stresses and strains are not fixed for non-proportional loading conditions (phase shift $\neq 0° \; or \; 180°$) and rotate during a cycle (rotating principal stresses and strains RPSS). These tests, called in the following RPSS tests, were performed at room temperature and 500°C.

4.3.1 Experimental details

The experimental setup used to perform the FPSS multiaxial fatigue tests consists of a commercial tension-torsion machine extended with a pressure vessel allowing the application of alternating circumferential load on tube specimen by maintaining the external pressure constant and varying the internal pressure [11][12]. A schematic view of the setup is illustrated in Figure 4-6. All FPSS tests were fully strain controlled with alternating axial and circumferential strains which are varied according sinusoidal courses with a frequency of 0.1 Hz and a circumferential strain amplitude equal the axial strain amplitude for all tests. The phase shift between the course of axial stain and the course of circumferential strain and the strain amplitudes selected belong to the test conditions which were varied from test to test. Table 4-2 shows the selected strain amplitudes for the chosen phase shifts.

Table 4-2: Nominal strain amplitudes [%] of FPSS multiaxial tests performed depending on the phase shift.

Phase Shift	0°	45°	90°	135°	180°
	0,13 0,14 0,15 0,17 0,17	0,12 0,14 0,15	0,14 0,15 0,16 0,17	0,16 0,18 0,20	0,18 0,20 0,22 0,24

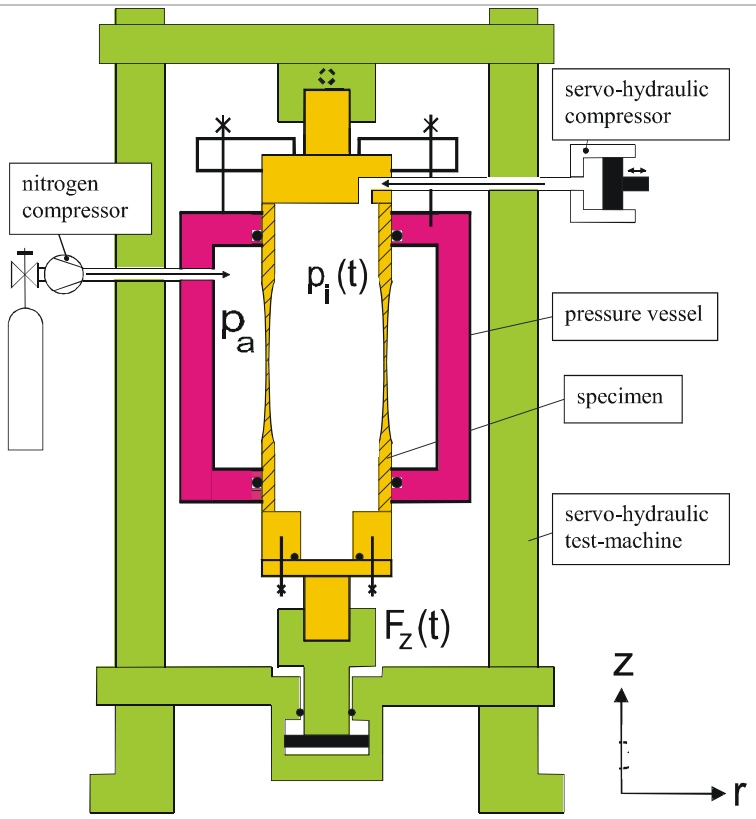

Figure 4-6 Schematic view of the biaxial test facility for tests with fixed directions of principal stresses and strains (FPSS) and its mechanical components

Since water is used as an incompressible medium for the internal pressure used, the setup is qualified for tests at room temperature only. Consequently FPSS multiaxial fatigue tests could not be performed at high temperatures and at these temperatures RPSS multiaxial fatigue tests were chosen instead.

The RPSS tests were conducted using the same testing machine skipping the pressure vessel and mounting a resistance furnace on the pillar of the biaxial testing machine (s. Fig. 4-7). To ensure that the clamping jaws are not heated, the bolts which are welded with the specimens were extended, so that is was able to mount cooling sleeves around. Furthermore we used a combined tension/torsion extensometer to measure the axial strain ε_{ax} and the shear strain γ simultaneously. All experiments were fully strain controlled with alternating axial and shear strains which are varied according sinusoidal courses with a frequency of 0.5 Hz and a shear strain amplitude equal the axial strain amplitude multiplied by $\sqrt{3}$ for all tests. Beside the temperature the phase shift between the course of axial stain and the course of shear strain as well as the strain amplitudes selected belong to the test conditions which may vary from test to test. Table 4-3 shows the selected strain amplitudes related to the selected phase shifts and temperatures for the performed experiments.

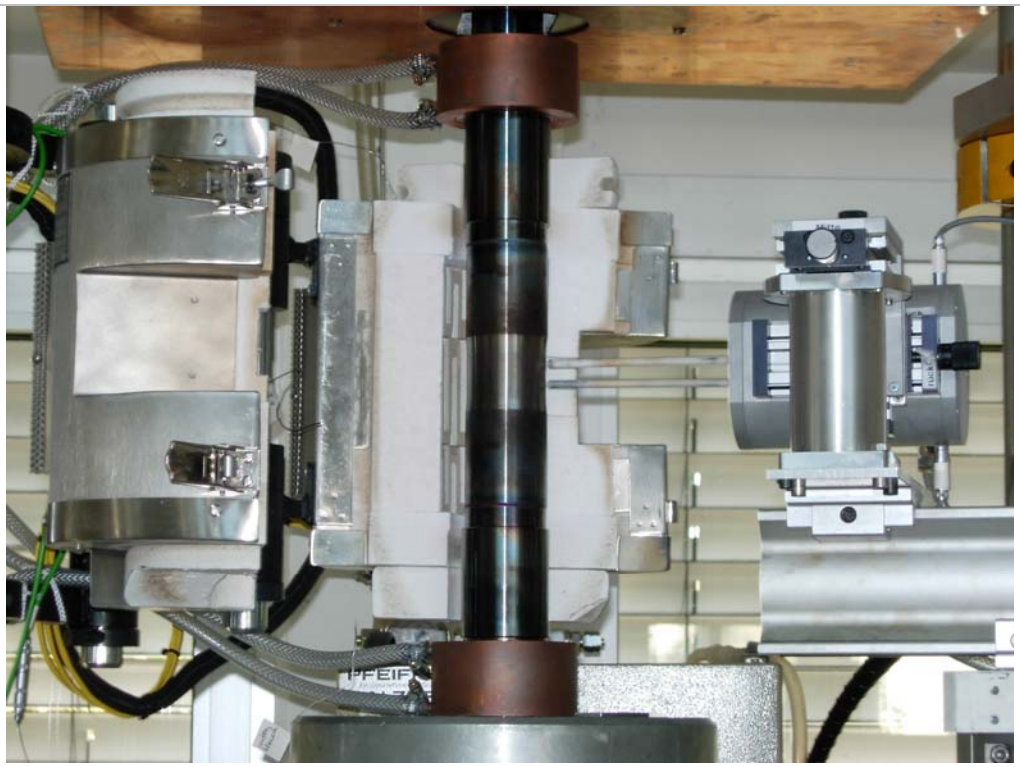

Figure 4-7 Biaxial test facility for RPSS tests (tension/torsion)

Table 4-3: Nominal axial strain amplitudes [%] of RPSS multiaxial tests, performed depending on the temperature and the phase shift.

Temperature	Phase Shift	0°	45°	90°	135°	180°
Room temperature		0,12 0,14 0,16 0,18 0,18	0,12 0,14 0,16 0,18	0,14 0,16 0,18	0,14 0,16 0,18	0,16 0,18 0,18 0,18
500°C		0,12 0,14 0,16	0,12 0,14 0,16	0,14 0,16 0,18	0,14 0,16 0,18	0,14 0,16 0,18

4.3.2 Experimental results

In the regime of low cycle fatigue the relevant parameter for failure is usually the inelastic strain amplitude. Therefore in a first evaluation we plotted in a Manson-Coffin diagram the equivalent inelastic strain range at half number of cycles to failure versus number of cycles to failure. The equivalent inelastic strain range is calculated using a similar procedure to that described in 2.2.2 (eq. 2.6) with the components of inelastic strain instead those of the total mechanical strain are considered.

The resulting plot for the FPSS experiments at room temperature can be seen in Figure 4-8 where the lifetime data depending on the phase shift are compared to those of uniaxial tests. It can recognized that the multiaxial loading with fixed directions of principal stresses and strains (FPSS) yields lower lifetimes in the low cycle fatigue regime with non-monotonous dependence on the phase shift. While the non-proportional multiaxial loading (phase shifts 45, 90 and 135°) seems to be the most damaging mode, the proportional multiaxial loading with 180° phase shift yields higher lifetimes, very close to those of the corresponding uniaxial loading, than the proportional multiaxial loading with 0° phase shift. In comparison to the uniaxial loading the multiaxial FPSS with the same equivalent inelastic strain range have led to up to 30 times lower lifetimes.

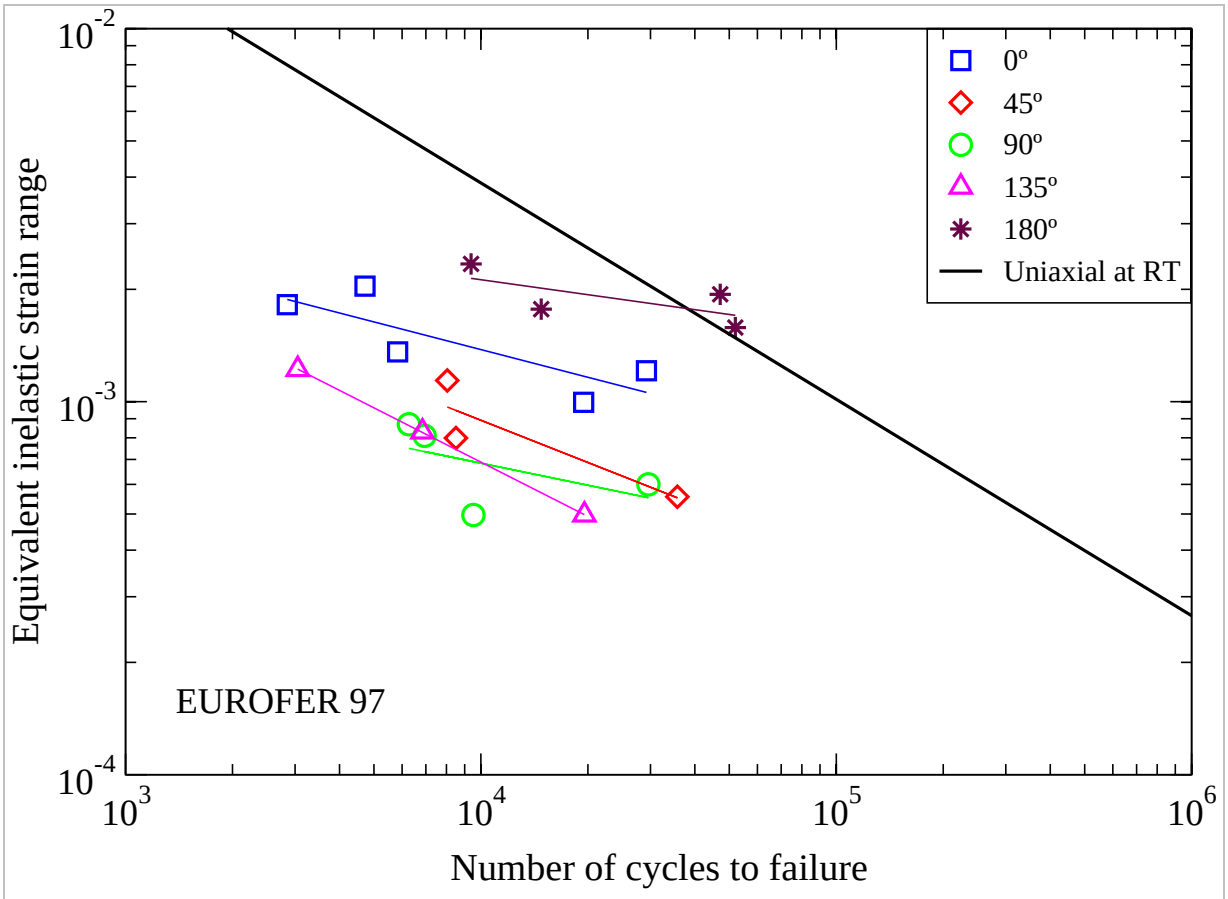

Figure 4-8 Equivalent inelastic strain range at half number of cycles to failure versus number of cycles to failure for the multiaxial FPSS tests performed at room temperature.

When considering the same plot for the RPSS tests at room temperature (s. Figure 4-9) similar decrease in the lifetime due to loading multiaxiality with however more or less same dependence on the phase shift. Comparing the lifetimes of RPSS tests with those of the FPSS tests for the same equivalent inelastic strain ranges, higher lifetimes can be recognized under RPSS multiaxial loading mode which anyhow could yield up to 15 times lower lifetimes than the corresponding uniaxial loading.

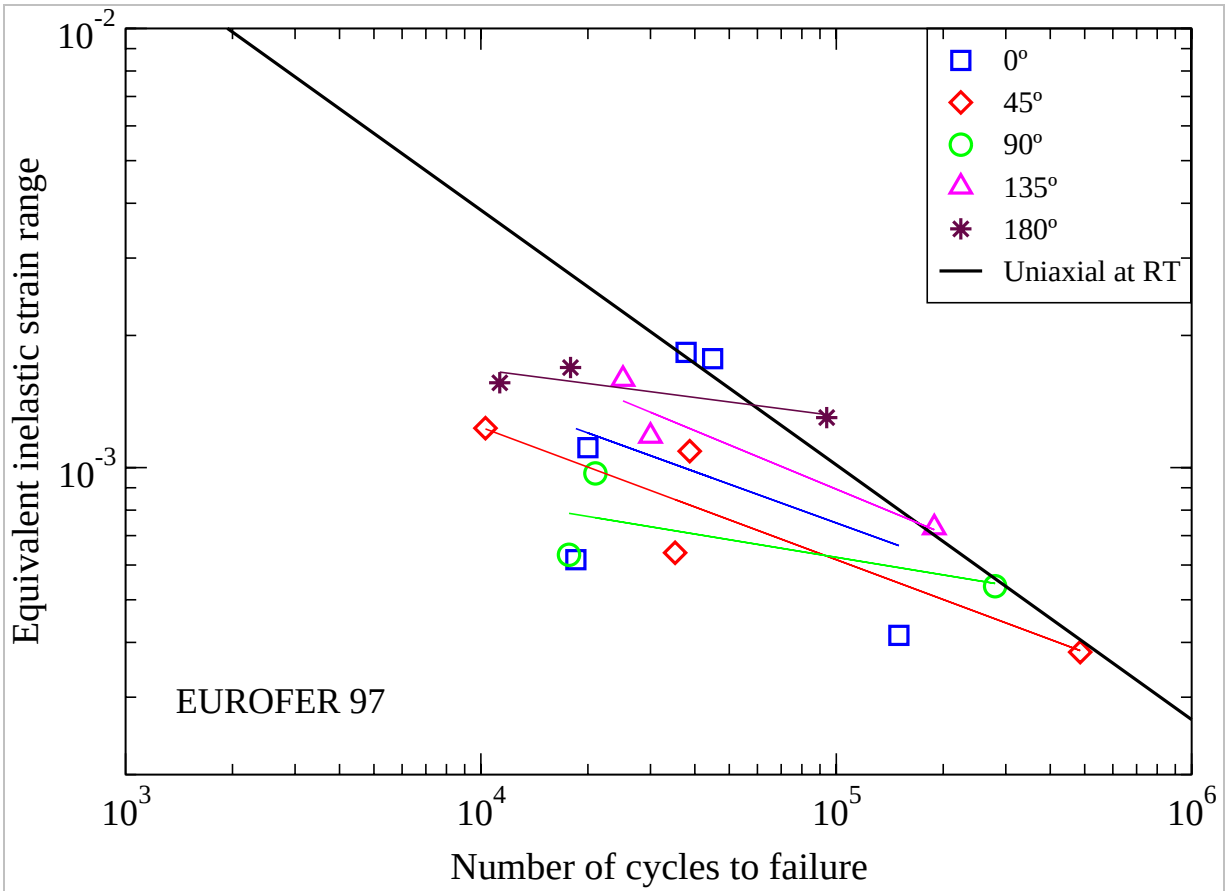

Figure 4-9 Equivalent inelastic strain range at half number of cycles to failure versus number of cycles to failure for the multiaxial RPSS tests performed at room temperature.

The high temperature RPSS tests at 500°C delivered also lifetimes lower than those under uniaxial loading (s. Figure 4-10) whereas the decrease in lifetime by a factor of up to 50 is much lower than that obtained from room temperature tests. In addition, there is no clear dependence of the fatigue lifetime on the phase shift which is however due to the much higher scatter hard to be identified.

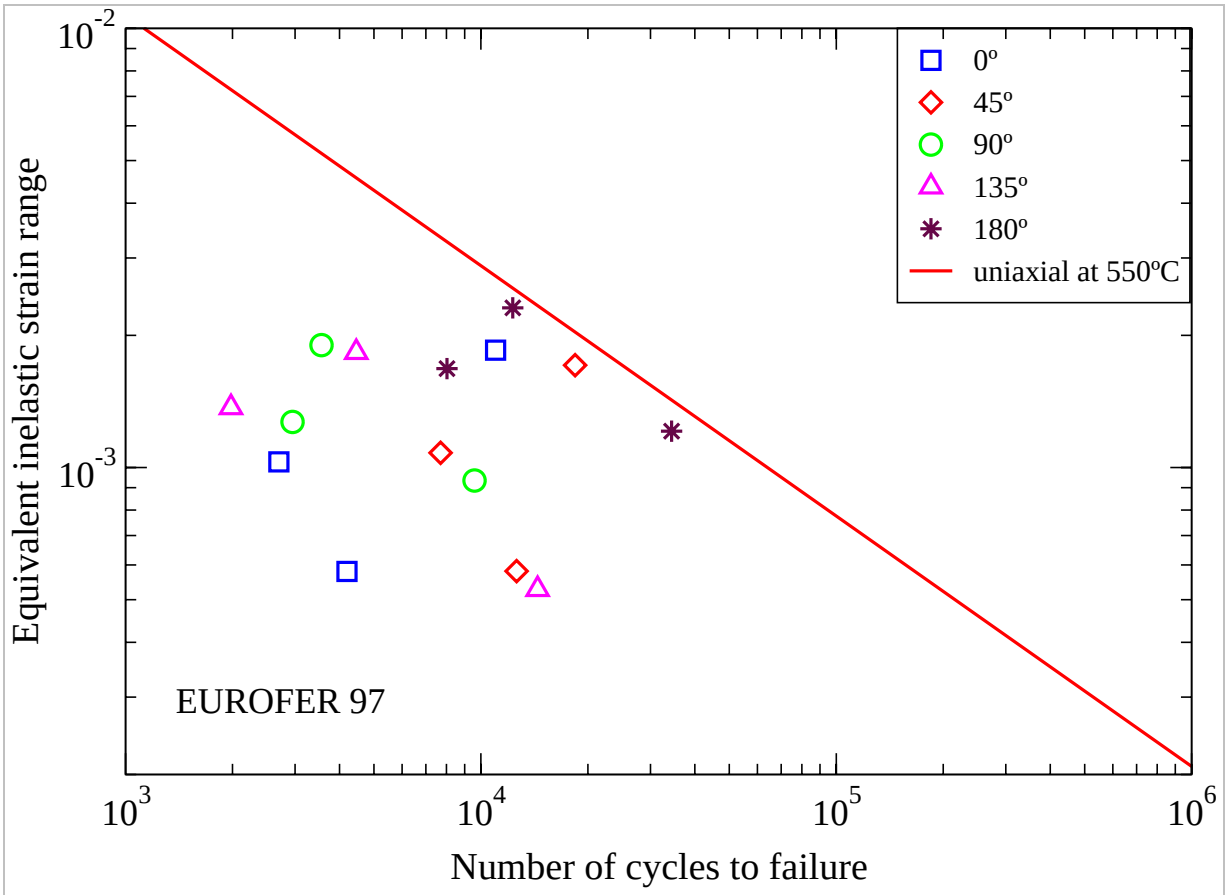

Figure 4-10 Equivalent inelastic strain range at half number of cycles to failure versus number of cycles to failure for the multiaxial RPSS tests performed at 500°C.

For further discussion the results of all multiaxial tests performed are summarized in Figure 4-11 where it can be recognized that there is not that clear correlation between equivalent inelastic strain range and number of cycles to failure for multiaxial loading like it is the case for uniaxial loading. Nevertheless the test results particularly those at room temperature show the common tendency, the higher the equivalent inelastic strain range is the lower is the fatigue lifetime. The apparent large scatter of the data is indeed mainly caused by the influence of the phase shift between the loadings in the different direction which results in different stress states [13]. Hence, the equivalent stress range at the same cycle (half number of cycles to failure) was viewed and plotted versus number of cycles to failure. As its can be seen in Figure 4-12 the FPSS loading causes shorter lifetimes than the RPSS loading with the same equivalent stress range (see Figure 4-12). Furthermore the correlation between equivalent stress range and number of cycles to failure for RPSS loading fits very well to that determined for the uniaxial loading (see Figure 4-12).

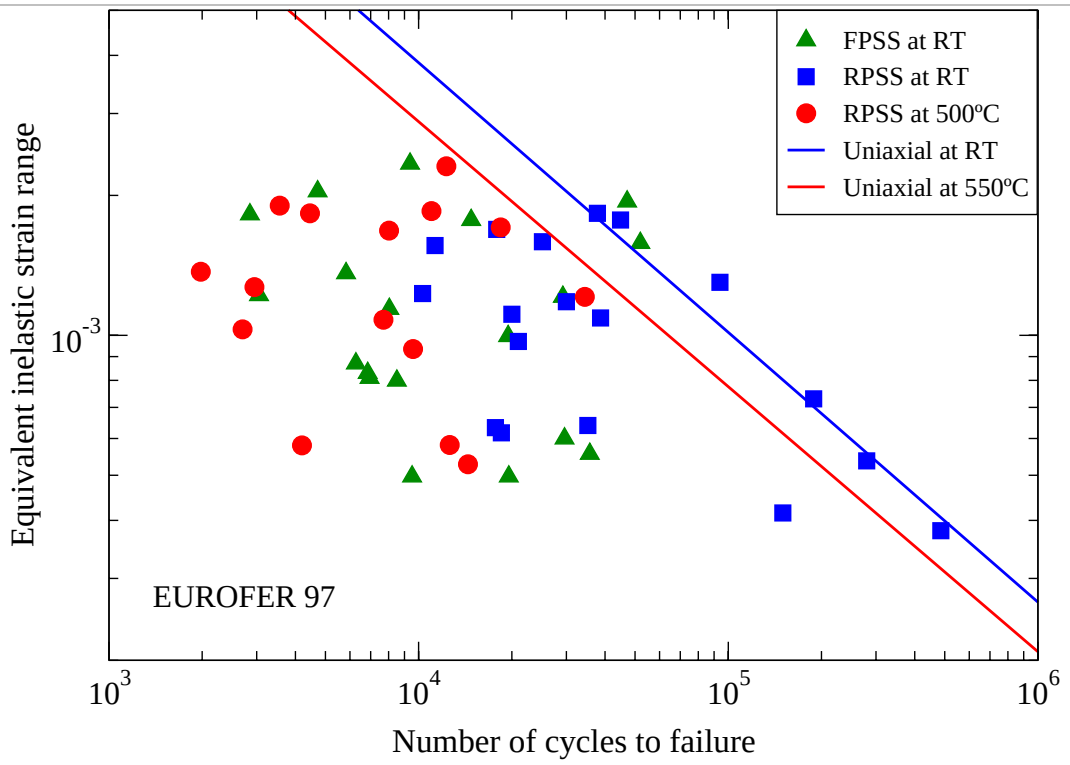

Figure 4-11 Equivalent inelastic strain range at half number of cycles to failure versus number of cycles to failure for the multiaxial tests performed.

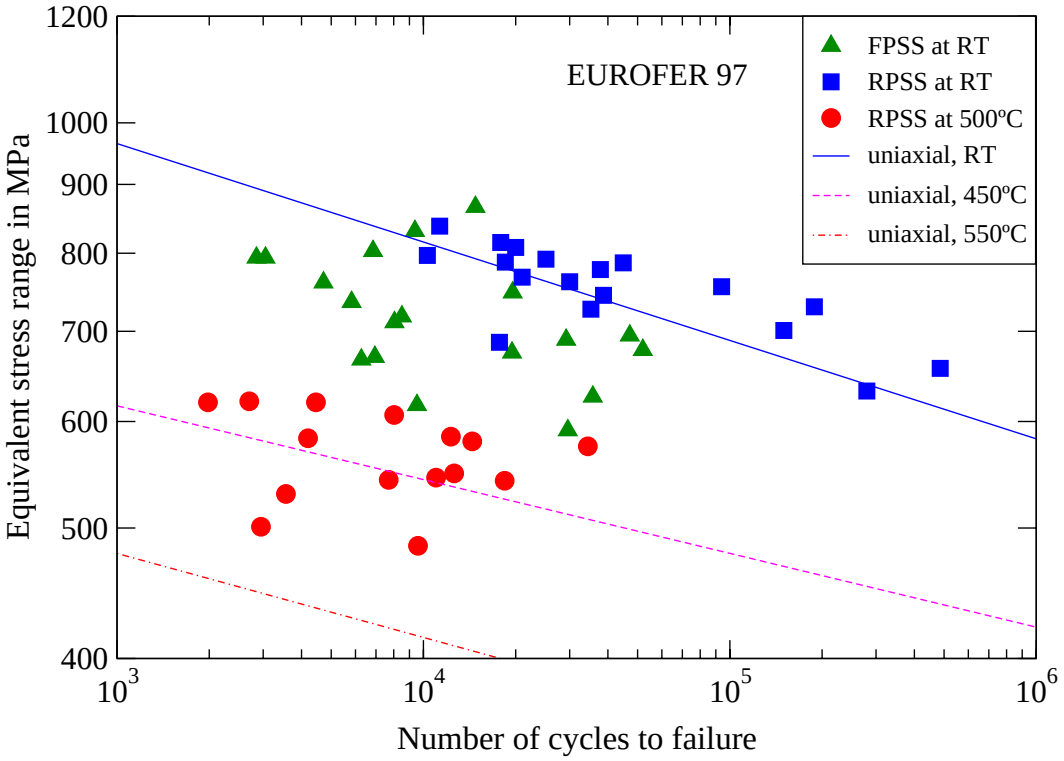

Figure 4-12 Equivalent stress range at half number of cycles to failure versus number of cycles to failure for the multiaxial tests performed and the uniaxial tests in comparison.

In conclusion both, inelastic strain and stress, affect damage and lifetime of EUROFER 97 under multiaxial loading, as it has been already verified under uniaxial loading [3]. The total strain, which is a linear combination of stress and inelastic strain, is not a sufficient parameter for representing both and their influences on lifetime as it can be seen on Figure 4-13. In Figure 4-13 the equivalent total strain range is plotted versus number of cycles to failure for the multiaxial tests performed. For comparison the corresponding design curves marking the numbers of allowable cycles as determined in section 3 for EUROFER 97 are plotted too. It can be seen that for the same mechanical strain range multiaxial loading yields number of cycles to failure even lower than the number of allowable cycles. Particularly, this is observed for one RPSS test and view FPSS tests at room temperature as well as for two RPSS tests at 500°C. Hence, the design curves, in spite of high safety factors included, are not sufficiently conservative. Consequently, conventional design rules considering fatigue and creep-fatigue interaction are not straightforward applicable to EUROFER 97.

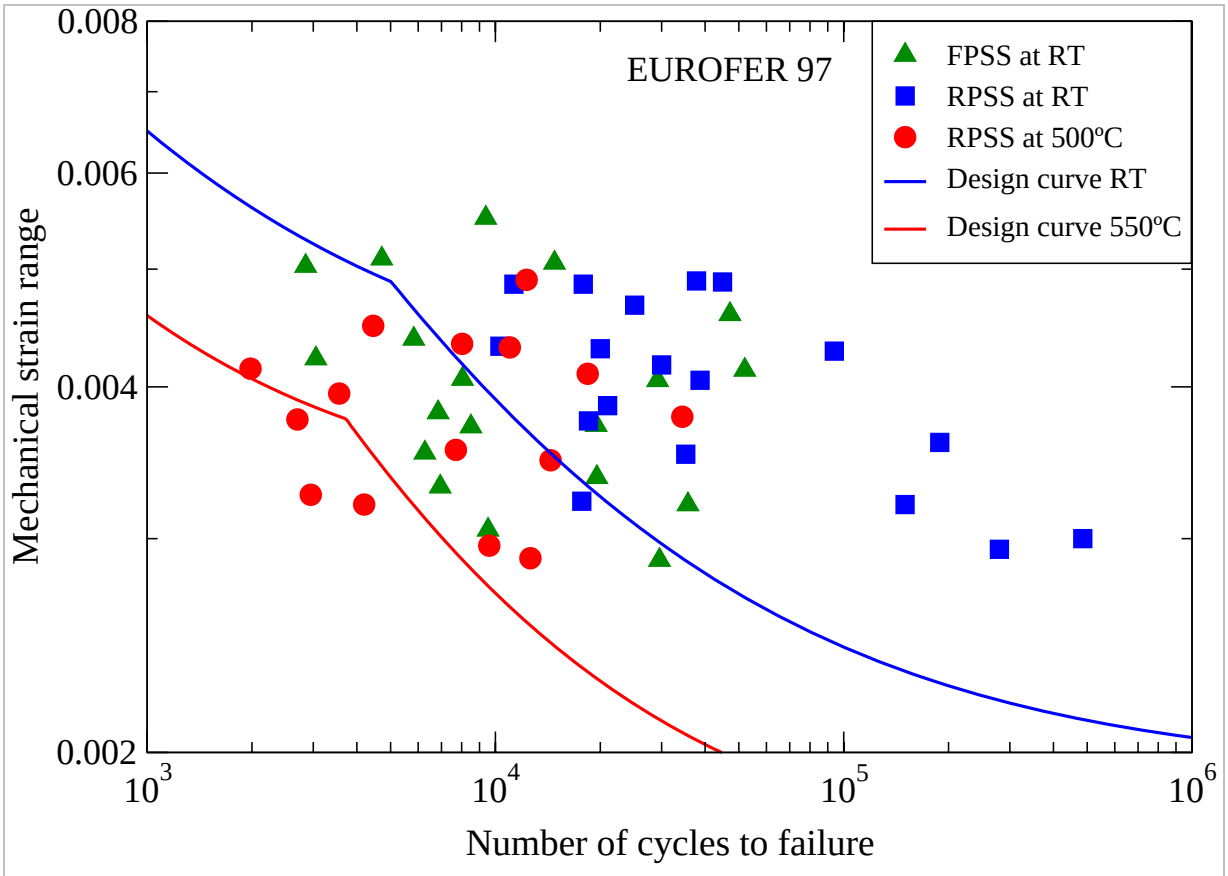

Figure 4-13 Equivalent total (mechanical) strain range versus number of cycles to failure for the multiaxial tests performed in comparison to the corresponding design curves identified for EUROFER 97 in section 3 (s. Figure 3-2), which mark the allowable number of cycles for a given mechanical strain range and vice versa.

5 Improved rules for EUROFER 97

Based on the results of the verification experiments evaluated and discussed above an improved rule for determining the allowable number of cycles and thus the fatigue damage part in eq. 2.1 has been developed within the EFDA task TW5-TTMS-005, D7.

Starting to gather physical interpretation why the multiaxial fatigue tests have delivered lifetimes lower than those expected on the base of uniaxial data we plotted the cyclic hardening curves (half of equivalent stress range versus half of equivalent strain range, both of the cycle at half number of cycles to failure) obtained from the multiaxial fatigue tests and compared them with those determined from uniaxial fatigue tests and with the monotonic hardening curves from uniaxial tensile tests as well (s. Figure 5-1). From Frigure 5-1 the following can be recognized:

1. In the multiaxial fatigue tests with rotating principal stresses and strains (RPSS tests) at room temperature and 500°C much lower softening is observed than that observed in uniaxial fatigue tests.

2. In the multiaxial fatigue tests with fixed directions of principal stresses and strains (FPSS tests) at room temperature a more pronounced softening is observed than that observed in RPSS tests, which however achieves for few tests the softening level observed in uniaxial fatigue tests.

Physically this can be explained by the following. Under RPSS multiaxial loading more glide systems are indeed activated but with result that the inelastic deformation localized in the different systems is smaller than that under uniaxial and FPSS loadings. Since localized deformation on the sub grain scale is necessary to break the carbides walls between the ferritic phases and former martensitic laths yielding softening reduced softening is observed under RPSS multiaxial loading. Obviously, such inelastic deformation localisations are more in favour under FPSS multiaxial loading and most in favour under uniaxial loading.

The low fatigue lifetimes observed in the multiaxial fatigue tests might be now, at least partly, attributed in the case of RPSS and FPSS multiaxial tests to the reduced softening and thus the higher stresses.

Based on these findings, the design fatigue curves for EUROFER 97 (Figure 3-2) are modified taking into account the cyclic softening and its dependence on the loading mode. Therefore we considered again the basis of these curves, namely the isothermal low cycle fatigue data of EUROFER 97 (mechanical strain range $\Delta\varepsilon$ vs. number of cycles to failure N_f) and derived there from the relation between the mechanical strain range $\Delta\varepsilon$ and the hypothetical number of cycles to failure N_f^* which would be observed in the absence of softening. To determine N_f^* the damage model already developed for EUROFER 97 under low cycle fatigue loading conditions is considered [3]. According to this model the damage accumulated per cycle during a cyclic loading has the following dependence on stress and inelastic strain ranges

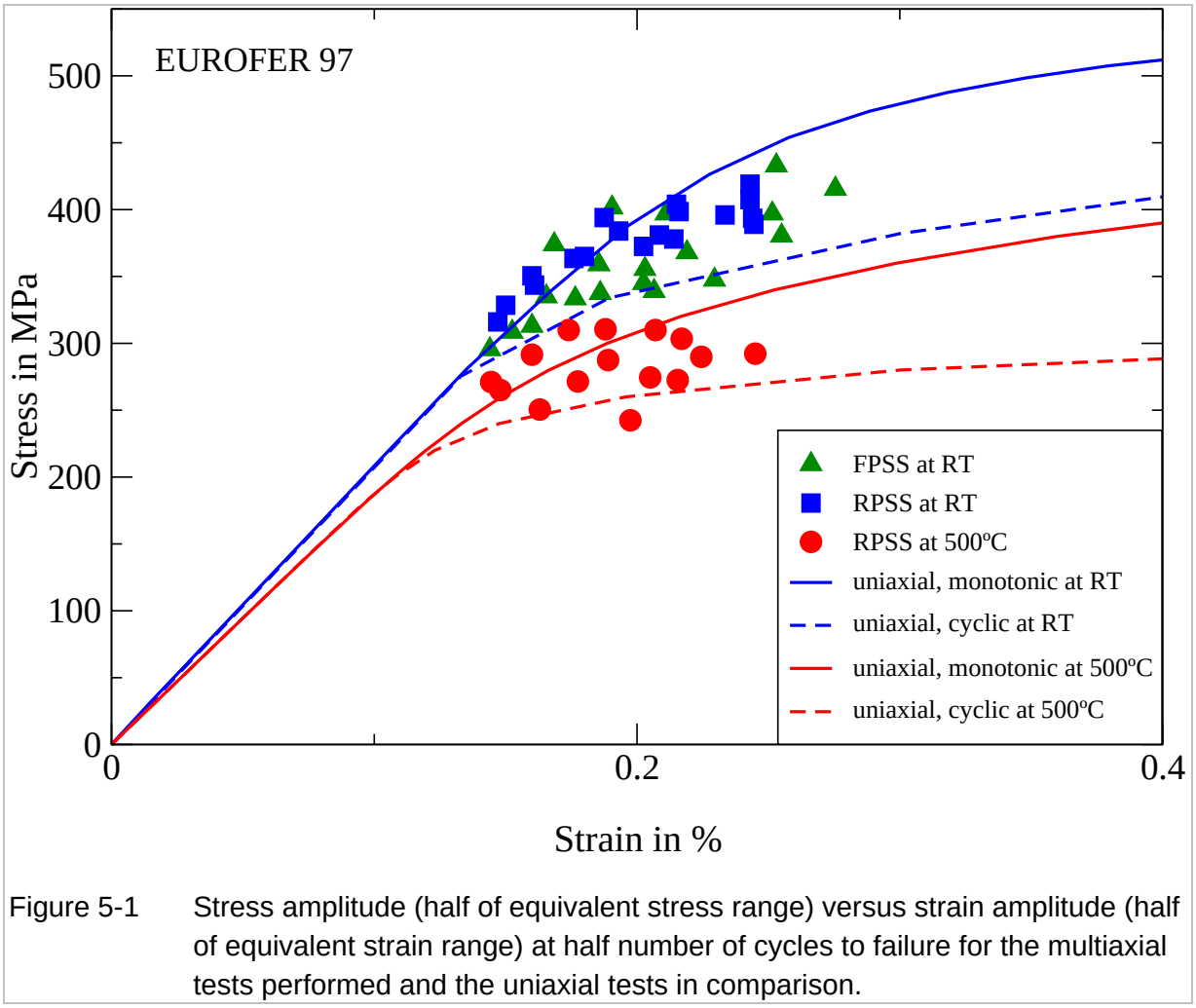

Figure 5-1 Stress amplitude (half of equivalent stress range) versus strain amplitude (half of equivalent strain range) at half number of cycles to failure for the multiaxial tests performed and the uniaxial tests in comparison.

$$\delta D \propto (\Delta\sigma)^r \, \Delta\varepsilon^{in} \tag{5.1}$$

with r as stress sensitivity exponent which is a temperature dependent parameter. Based on eq. 5.1 the following results for N_f:

$$N_f \propto \left(\Delta\sigma\right)^{-r} \left(\Delta\varepsilon^{in}\right)^{-1} \tag{5.2}$$

With eq. 5.2 the value of N_f^* for a given isothermal uniaxial low cycle fatigue test can be determined as:

$$N_f^* = N_f \left(\frac{\Delta\sigma_{N_f/2}}{\Delta\sigma_{1st\,cycle}} \right)^r \frac{\Delta\varepsilon^{in}_{N_f/2}}{\Delta\varepsilon^{in}_{1st\,cycle}} \tag{5.3}$$

$\Delta\sigma_{1st\,cycle}$ and $\Delta\sigma_{N_f/2}$ are the stress ranges of the first cycle and the cycle at half number of cycles to failure, respectively, and $\Delta\varepsilon^{in}_{1st\,cycle}$ and $\Delta\varepsilon^{in}_{N_f/2}$ denote the inelastic strain ranges of these cycles. Using eq. 5.3 the values of N_f^* have been determined for the isothermal uniaxial low cycle fatigue tests performed with different $\Delta\varepsilon$ at different temperatures. Thereby the values of r, published in [3] for EUROFER 97 at 450 and 550°C, were considered. The value of r at room temperature was extracted considering the relations $\Delta\varepsilon^{in}_{N_f/2} = \alpha \, N_f^{\,\beta}$ and

$\Delta\sigma_{N_f/2} = p\,\Delta\varepsilon^{in}_{N_f/2}{}^{q}$ fitted to the isothermal fatigue data at room temperature. After determining the values of N_f^*, the relation between $\Delta\varepsilon$ and N_f^* has been described by fitting the following relation to the data obtained:

$$\Delta\varepsilon = b_1 + b_2 N_f^{*\,b_3} \tag{5.4}$$

The resulting values of the temperature dependent parameters b_1, b_2 and b_3 are listed in Table 5-1. Based on this relation new design fatigue curves (mechanical strain range $\Delta\varepsilon$ vs. number of allowable cycles N_d) have been derived by applying the appropriate factors (refer to section 2.3):

$$\Delta\varepsilon = \min\left\{0.5\left(b_1 + b_2 N_d^{b_3}\right),\ b_1 + b_2\left(20 * N_d\right)^{b_3}\right\} \tag{5.5}$$

The new fatigue design curves are plotted in Figure 5-2.

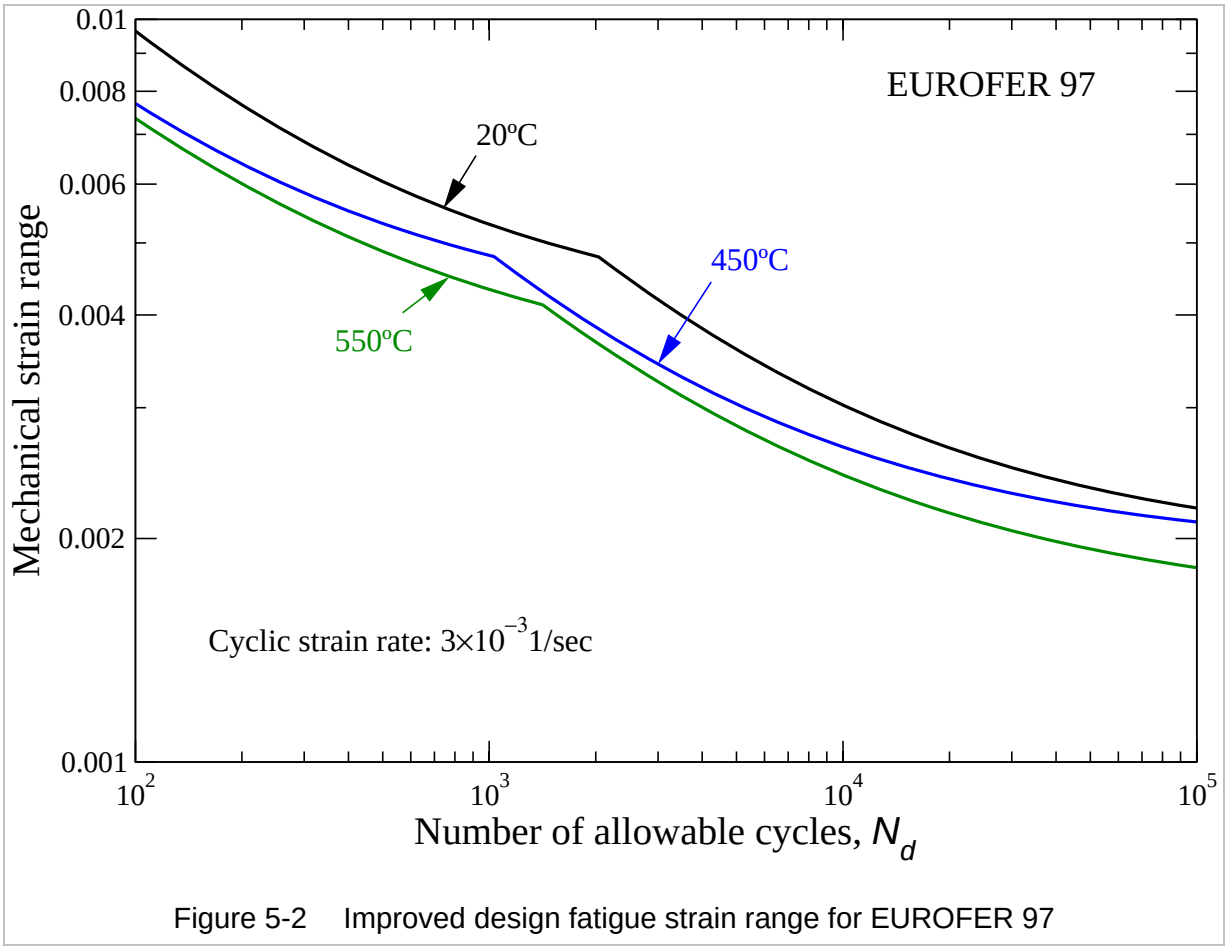

Figure 5-2 Improved design fatigue strain range for EUROFER 97

When comparing the allowable numbers of cycles determined by the new fatigue design curves with the numbers of cycles to failure observed in the most critical verification tests, namely the multiaxial tests reported in the previous section, improved reliability with the new fatigue design curves can be noticed. Almost all verification tests yield higher fatigue lifetimes than those would be allowed by the new fatigue design curves for components under fatigue loading (s. Figure 5-3). However, since for few tests the number of cycles to failure is very

close to the allowable number of cycles further verification of the new fatigue design curves might be necessary.

Table 5-1: Parameters of equation 3.2 determined for EUROFER 97

Temperature in °C	b_1	b_2	b_3
20	3.84×10^{-3}	0.56	-0.60
450	3.84×10^{-3}	0.36	-0.60
550	3.2×10^{-3}	0.31	-0.56

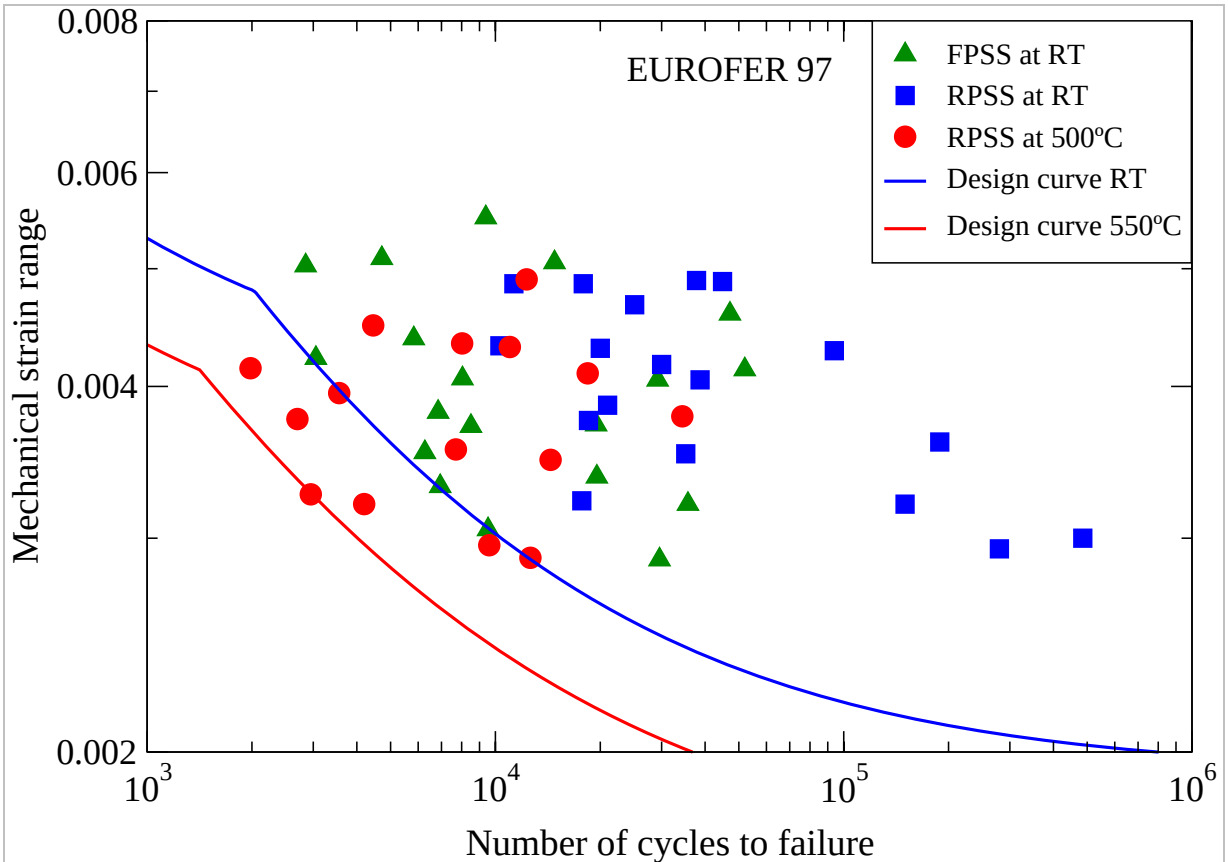

Figure 5-3 Equivalent total (mechanical) strain range versus number of cycles to failure for the multiaxial tests performed in comparison to the corresponding improved design curves for EUROFER 97, which mark the allowable number of cycles for a given mechanical strain range and vice versa.

6 Summary and outlook

In this report the creep-fatigue design rules already established in the ASME and RCC-MR codes have been reviewed, evaluated and reformulated for the assessment of components built from EUROFER 97. Therefore creep and fatigue data of EUROFER 97 were processed deriving the required design curves which were described in addition by analytical formula. For the allowable sum of creep fatigue damage the most conservative values proposed in the ASME code were adopted in a first approach.

To verify the rules, particularly those for fatigue, an extensive experimental program has been conducted in which isothermal two steps LCF, thermo-mechanical fatigue and isothermal multiaxial fatigue experiments were performed. The results of these experiments showed that the thermo-mechanical and multiaxial loading modes are much more damaging than the uniaxial loading. The observed fatigue lifetimes for the same equivalent loads are much lower than the uniaxial references and in many cases lower than those allowed by the formulated design rules. This characteristic behaviour for EUROFER 97, and probably for all similar ferritic martensitic steels, has been attributed in a deeper evaluation of the verification experiments to the cyclic softening behaviour of this material. The cyclic softening has been found less pronounced under thermo-mechanical and multiaxial fatigue loading and most pronounced under isothermal uniaxial fatigue loading yielding lower stresses in strain controlled loadings and thus higher lifetimes. As a consequence, the fatigue design curves derived from uniaxial fatigue data are not sufficiently conservative. In addition, the simulations performed for the thermo-mechanical fatigue tests showed that cyclic softening leads to deformation localisation which might also contribute to the lifetime reduction. The non-proportionality (phase shift) under multiaxial fatigue loading has also been found to have negative influence on the lifetime.

To improve the reliability of the rules, new fatigue design curves were derived taking into account the influence of reduced cyclic softening on lifetime. Therefore, a damage model recently developed to describe the deterioration of EUROFER 97 under creep fatigue loading has been used. However, even the new design curves cover reliably the lifetimes observed in the verification experiments performed so far further verifications are recommended, particularly considering the lifetimes of the following types of experiments:

1. Isothermal multiaxial fatigue tests with higher loading amplitudes – using specimen with improved buckling behaviour – at room as well as at high temperatures

2. Isothermal LCF tests with long dwell periods (up to hours) for the verification of assumed allowable creep fatigue summations

3. Thermo-mechanical fatigue tests on different specimen geometries for the investigation of the deformation localisation effects due to cyclic softening on the lifetime

4. A benchmark experiment in which a mockup built from EUROFER 97 will be tested under thermo-mechanical multiaxial creep fatigue conditions.

7 Acknowledgment

We would like to thank Dipl.-Ing. S. Knaak, M. Klotz and Dipl.-Ing. M. Lerch, members of our scientific technical stuff, for their support in performing the verification experiments.

This work, supported by the European Communities under the contract of Association between EURATOM and Forschungszentrum Karlsruhe, was carried out within the framework of the European Fusion Development Agreement. The views and opinions expressed herein do not necessarily reflect those of the European Commission.

8 References

[1] B. van der Schaaf, F. Tavassoli, C. Fazio, E. Rigal, E. Diegele, R. Lindau and G. LeMarois, The development of EUROFER reduced activation steel, Fusion Engineering and Design 69 (2003) 197-203.

[2] ITER Structural Design Criteria for In-Vessel Components (SDC-IC), G 74 MA 8 01-05-28 W 0.2.

[3] J. Aktaa and R. Schmitt, High temperature deformation and damage behavior of RAFM steels under low cycle fatigue loading: Experiments and modeling, Fusion Engineering and Design 81 (2006) 2221-2231.

[4] B.F. Langer, Design of pressure vessels for low cycle fatigue, J. Basic Engg. 84 (1962) 379-.

[5] F. Tavassoli, Fusion Demo Interim Design Criteria (DISDC) / Appendix A: Material Design Limit Data / A3.S18E Eurofer Steel, DMN Technical Report, DMN/DIR/NT/2004-000/A, 2004.

[6] M. Schirra, A. Falkenstein, P. Graf, S. Heger, H. Kempe, R. Lindau, H. Zimmermann, Ergebnisse von Charakterisierungsuntersuchungen zu physikalischen und mechanischen Eigenschaften des martensitischen 9 % Cr-Stahls EUROFER 97, FZKA-Bericht 6707, 2002.

[7] M. A. Miner, Cumulative Damage in Fatigue, Journal of Applied Mechanics, ASME, Vol. 12, No. 3, A159-A164, Sept. 1945.

[8] C. Petersen, Thermal fatigue behavior of low activation ferrite-martensite steels, Journal of Nuclear Materials 258-263 (1998) 1285-1290.

[9] D. A. Miller and R. H. Priest, in High Temperature Fatigue: Properties and Prediction, ed. R. P. Skelton, Elsevier Applied Science, pp. 113-175, 1987.

[10] J. Aktaa, M. Klotz and C. Petersen, Deformation and Damage of RAFM Steels under Thermo-Mechanical Loading: A Challenge for Constitutive Equations, Journal of Nuclear Materials 367-370 (2007) 550-555.

[11] B. Windelband, B. Schinke and D. Munz, Determination of strain components in low-cycle multiaxial fatigue tests on tubes, Nuclear Engineering and Design 162 (1996) 47 -53.

[12] M. Weick and J. Aktaa, Mehrachsige Ermüdungsprüfung an Rohrproben – Untersuchung des Ermüdungsverhaltens unter mehrachsiger nichtproportionaler Belastung, Materialprüfung 45 (2003) 371-374.

[13] M. Weick & J. Aktaa, "Microcrack propagation and fatigue lifetime under non-proportional multiaxial cyclic loading," International Journal of Fatigue 25 (2003) 1117-1124.